Figure 4

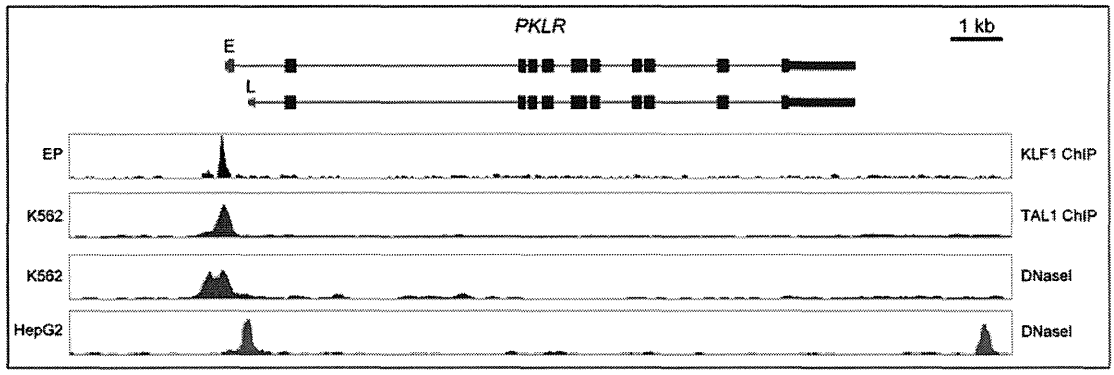

J Clin Immunol
DOI 10.1007/s10875-013-9964-4

ASTUTE CLINICIAN REPORT

Allogeneic Bone Marrow Transplantation Appears to Ameliorate IgA Nephropathy in a Patient with X-linked Thrombocytopenia

Akihiro Hoshino · Masaki Shimizu · Hiroyoshi Matsukura · Hisano Sakaki-Nakatsubo · Keiko Nomura · Toshio Miyawaki · Hirokazu Kanegane

Received: 24 February 2013 / Accepted: 29 October 2013

Abstract Wiskott-Aldrich syndrome (WAS) is caused by a mutation in the *WAS* gene, and it is clinically characterized by the triad of thrombocytopenia, eczema and immunodeficiency. X-linked thrombocytopenia (XLT), which is a clinically mild form of WAS, is also caused by a *WAS* gene mutation. Patients with WAS/XLT sometimes also have autoimmune diseases such as IgA nephropathy. Progression of IgA nephropathy may lead to chronic renal failure with a poor prognosis. Here, we describe an XLT patient who also had IgA nephropathy. The patient underwent bone marrow transplantation (BMT) because of an associated-lymphoproliferative disorder, and clinical and histological improvement in his IgA nephropathy was observed after BMT. The amount of galactose-deficient IgA in the patient's serum markedly decreased after BMT. Therefore, immunological reconstitution might improve autoimmune diseases in patients with WAS/XLT.

Keywords Aberrant IgA · bone marrow transplantation · IgA nephropathy · Wiskott-Aldrich syndrome · X-linked thrombocytopenia

A. Hoshino · H. Sakaki-Nakatsubo · K. Nomura · T. Miyawaki · H. Kanegane (✉)
Department of Pediatrics, Graduate School of Medicine and Pharmaceutical Sciences, University of Toyama, 2630 Sugitani, Toyama 930-0194, Japan
e-mail: kanegane@med.u-toyama.ac.jp

M. Shimizu
Department of Pediatrics, School of Medicine, Institute of Medical, Pharmaceutical and Health Sciences, Kanazawa University, Kanazawa, Japan

H. Matsukura
Department of Pediatrics, Saiseikai Toyama Hospital, Toyama, Japan

Published online: 12 November 2013

Introduction

Wiskott-Aldrich syndrome (WAS) is clinically characterized by thrombocytopenia with small platelets, eczema, and humoral and cellular immunodeficiency, and it is caused by a mutation in the *WAS* gene and deficient expression of WAS protein (WASP) [1]. The molecular defect in *WAS* also results in X-linked thrombocytopenia (XLT), which is a clinically mild form of WAS [2]. Patients with WAS exhibit an increased incidence of autoimmune diseases, in which vasculitis, autoimmune hemolytic anemia and kidney disease are the most common manifestations [3]. Recently, a study involving a large cohort of patients with XLT revealed that autoimmune diseases are also frequently observed in XLT [4].

Kidney disease, the majority of which is IgA nephropathy, is found in 4–19 % and 5 % of patients with WAS [3, 5] and XLT [4], respectively. IgA nephropathy is a glomerulonephritis that is immunohistochemically characterized by mesangial proliferation with diffuse IgA deposition [6]. Multiple pathogeneses of IgA nephropathy, including impaired response to mucosal antigens, delayed clearance of immune complexes from the circulation and abnormal interaction with mesangial IgA receptors, have been reported [7]. In the above hypotheses, abnormal glycosylation of the IgA1 molecule plays a critical role [6, 7]. The level of poorly galactosylated IgA1 in serum was found to be increased in patients with IgA nephropathy [8]. Aberrant IgA had an increased tendency to self-aggregate and form immune complexes with IgG antibodies, and it is therefore more likely to be deposited in the mesangium [6]. In *WASP*-deficient mice, the increased production of aberrant IgA was strongly related to the development of IgA nephropathy [9].

The reason that aberrant IgA is produced in WAS/XLT remains unclear, but immunological dysfunction may play an important role [10–12]. Therefore, there is a possibility

that immune reconstitution improves IgA nephropathy. Our XLT patient demonstrated clinical and histochemical improvement in IgA nephropathy following bone marrow transplantation (BMT).

Material and Methods

Patient

The patient is a 19-year-old male, and he developed a subcutaneous hematoma at the age of 3 years, and was found to have thrombocytopenia. The family history showed that his maternal uncle had thrombocytopenia and IgA nephropathy, which resulted in end-stage renal failure at the age of 30 years. At the age of 6 years, the patient was diagnosed as having an XLT (G1487A).

Subsequently, he remained well, and his platelet count fluctuated between 50 and $100 \times 10^3/\mu L$. At the age of 8 years, the patient showed gross hematuria and proteinuria after an upper respiratory infection and was suspected to have glomerulonephritis (Table I). A percutaneous renal biopsy was performed, and he was diagnosed with IgA nephropathy [13]. He was treated with an angiotensin-converting enzyme inhibitor and low-dose prednisolone (PSL) for one year. He improved only partially, and the hematuria and proteinuria persisted. At the age of 14 years, he contracted an Epstein-Barr virus-negative atypical lymphoproliferative disorder and achieved remission after receiving 1 mg/kg per day of PSL.

Following the remission of lymphoproliferative disease, the patient underwent a BMT from an unrelated human leukocyte antigen (HLA)-matched donor. The pre-BMT conditioning regimen included busulfan (12.8 mg/kg), cyclophosphamide (200 mg/kg), rituximab (375 mg/m^2) and 3 Gy of total body irradiation. Tacrolimus (day -1 to 30, 0.01 mg/kg/day administered with continuous infusion, target serum levels of 10–15 ng/mL; from day 31 converted to oral at 0.03 mg/kg/day, target trough serum levels of 5 ng/mL), methotrexate (day 1, 15 mg/m^2; day 3, 10 mg/m^2) were used for graft-versus-host disease (GVHD) prophylaxis. Tacrolimus was tapered from 12 months after BMT and discontinued 20 months after BMT. PSL (0.2–0.5 mg/kg/day) was used for engraftment syndrome and GVHD for 8 months. The patient had complete chimerism soon after BMT. A second renal biopsy was performed 24 months after BMT (Table I).

Measurement of Lectin-Binding Serum IgA Levels

To examine the terminal galactosylation of IgA molecules, we used lectin-binding assays with Helix aspersa (HAA), which

Table I Laboratory findings of patient 1 before and after BMT

Test	At the first biopsy	1 year after low-dose PSL	Just before HSCT	At the second biopsy	Value
WBC	12,110	8,280	8,020	7,220	/μL
RBC	431	436	487	472	$\times 10^4/\mu L$
Hemoglobin	13.9	12.4	14.5	14.5	g/dL
Hematocrit	39.1	35.4	41.6	42.4	%
Platelets	82	49	158	232	$\times 10^3/\mu L$
BUN	9	10	14	7	mg/dL
Creatinine	0.5	0.5	0.8	0.6	mg/dL
IgG	613	916	899	1,060	mg/dL
IgA	264	315	261	131	mg/dL
IgM	23	18	116	267	mg/dL
CH50	34	NE	NE	NE	U/mL
C3	105	NE	NE	NE	mg/dL
C4	35	NE	NE	NE	mg/dL
Urinalysis					
Protein	2+	2+	2+	neg	
Occult blood	3+	+	+	neg	
RBC	100-150/HPF	10-19/HPF	10-19/HPF	neg	
WBC	5-10/HPF	5-10/HPF	neg	neg	
Hyaline cast	+	neg	neg	neg	
Granular cast	+	neg	1-4/WF	1-4/WF	

WBC white blood cells, *RBC* red blood cells, *BUN* blood urea nitrogen, *Ig* immunoglobulin, *CH50* complement activity, *NE* not examined, *C* complement, *HPF* high power field, *WF* whole field

recognizes terminal N-acetylgalactosamine (GalNAc) residues [14]. The ratio of the absorbance at 450 nm between IgA bound to HAA and total IgA (HAA/IgA) was calculated. The amount of galactose-deficient IgA in serum was estimated using the following formula: serum IgA concentration (C_{IgA})×HAA/IgA ratio.

Results

The first renal biopsy revealed that all of 28 glomeruli showed diffuse mesangial hypercellularity, and 4 glomeruli were completely scarred-in (Fig. 1a). Immunofluorescence studies showed IgA and IgG deposits were present, mainly in the mesangium (Fig. 1b and c). Electron microscopy showed a cluster of electron-dense deposits in the mesangium (Fig. 1g). The second renal biopsy showed that all 14 glomeruli were normal without mesangial proliferation, although 2 glomeruli showed mesangial sclerosis (Fig. 1d). IgA and IgG deposits significantly improved in immunofluorescent studies (Fig. 1e and f). Electron microscopy confirmed the disappearance of electron-dense deposits (Fig. 1h).

The IgA-dominant immune deposits in the mesangium and glomerular injury in the patient significantly improved after BMT. The amount of galactose-deficient IgA in his serum also markedly decreased after BMT (before BMT; 126.4 mg/dL, after BMT; 36.6 mg/dL) [14].

Discussion

This may be the first report to provide a detailed description of IgA nephropathy associated with WAS/XLT after BMT. The clinical course of the patient indicates that BMT can improve the IgA nephropathy associated with WAS/XLT. Although the detail was not described, a patient with IgA nephropathy and chronic myelogenous leukemia has been reported who had a remission not only of the leukemia but also of the IgA nephropathy after BMT [15]. In murine models of IgA nephropathy, IgA deposition in the glomerular lesion decreased after BMT from quiescent murine [16]. Conversely, BMT from the onset murine to quiescent murine resulted in IgA deposition in the glomerular lesion [17]. This study suggests that hematopoietic stem cells or their differentiated cells are related to IgA nephropathy. Recently, abnormalities of lymphocytes, which may be related to the production of aberrant IgA, have been reported [18–24]. B cells show abnormal activity of β-1,3-galactosyltransferase or α-2,6-sialyltransferase, which is the enzyme associated with glycosylation of the IgA1 molecule [18–20] and abnormal regulation of Toll-like receptors [21,

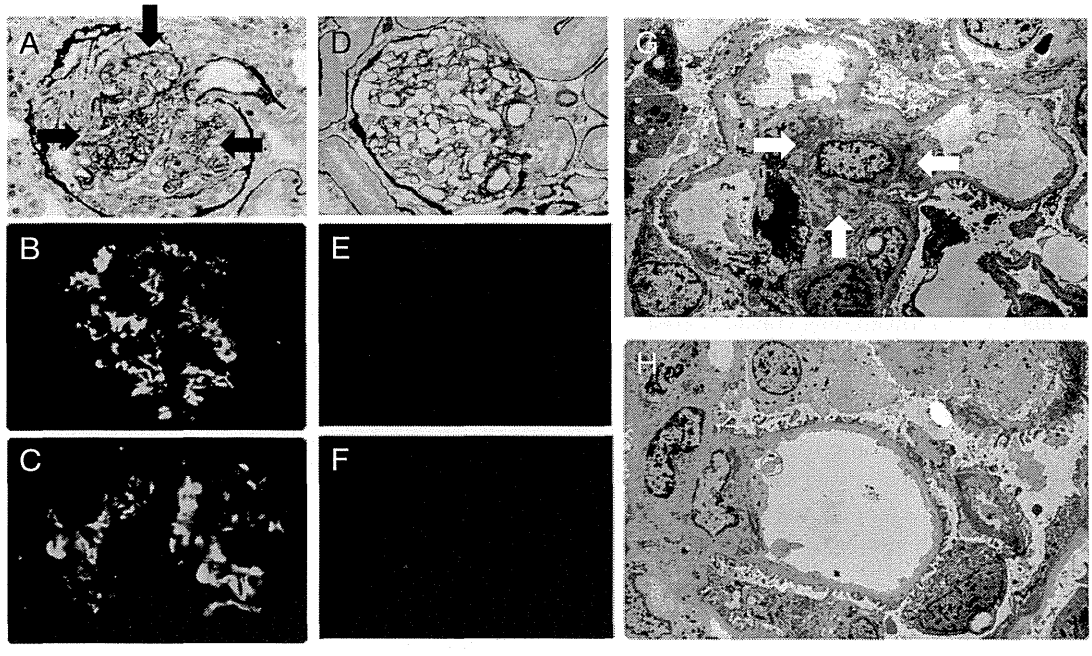

Fig. 1 Histological findings of renal biopsy samples from patient 1 before and after BMT. Histology of renal biopsy before (**a**, **b**, **c** and **g**) and after BMT (**d**, **e**, **f** and **h**). Periodic acid-methenamine-silver staining (**a** and **d**). Immunofluorescence studies of IgA (**b** and **e**) and IgG (**c** and **f**). Electron microscopy (**g** and **h**). Diffuse mesangial proliferative glomerulonephritis was observed (*arrows*) (**a**), and IgA and IgG deposits were observed in the mesangium (**b** and **c**) before BMT. Electron microscopy showed a cluster of electron-dense deposits in the mesangium (*arrows*) (**g**). Little proliferation of mesangium and cells was observed (**d**), and IgA, IgG and electron-dense deposits disappeared (**e**, **f** and **h**) after BMT

22]. T cells show abnormal secretion of IL-17 and T helper (Th) 2 cytokines in IgA nephropathy [19, 23].

The reason for the production of aberrant IgA and the development of IgA nephropathy in WAS/XLT remains unclear, but abnormalities of lymphocytes may play an important role. Consistent with previous reports, decreased levels of aberrant IgA and improvement of IgA nephropathy after BMT were observed in this patient. It has been reported that aberrant IgA and B cells which produce aberrant IgA increase age-dependently [9, 14], but there are no reports of mechanisms responsible for the aberrant glycosylation of IgA in WAS patients. However, impaired function of natural regulatory T cells and imbalance of Th1/Th2 cytokines, which are shown in IgA nephropathy, are also shown in WAS patients [10–12].

Histological improvement of IgA nephropathy might be caused by the clearance of mesangial IgA and the prevention of new IgA deposits. In renal transplantation, the deposits of mesangial IgA rapidly disappear after transplantation from donors with IgA nephropathy into recipients with non-IgA related disease [24, 25]. These observations seem to reflect a similar histological improvement. However, the precise mechanism remains unclear.

We suggest that hematopoietic stem cell transplantation (HSCT) for XLT patients can improve the long-term renal prognosis. HSCT at an early age is the treatment of choice for WAS patients [1]. However, therapeutic options for patients with XLT are controversial because of the excellent survival [4]. However, patients with XLT show a high rate of severe disease-related complications, and the prevalence of IgA nephropathy is 5 %; this condition occurs more frequently in Japanese patients, in whom the rate is 18 % [4]. Autoimmune diseases are significantly related to mixed/split chimerism for patients with WAS/XLT, suggesting that residual host lymphocytes or altered cytoskeleton can cause autoimmune diseases [26]. Therefore, adequate myeloablation and immunosuppression may be required.

Animal studies and the success in our patient support that HSCT may improve IgA nephropathy. Although in our patient, we cannot fully exclude the benefit of the myeloablative chemotherapy and post-transplant immunosuppressive GVHD-prophylaxis medications. Further studies are needed to define the role of the affected immune system in XLT and WAS in promoting IgA nephropathy, as well as, the role of immune reconstitution in improvement of the disease. Regardless, based on the supporting data from animal studies and our patient's beneficial result, HSCT should be considered for improving the clinical outcome in patients with XLT and IgA nephropathy.

Acknowledgments This study was supported by Grants-in-Aid for Scientific Research from the Ministry of Education, Culture, Sports, Science and Technology (to H. K. and T. M.), and grants from the Ministry of Health, Labour and Welfare of Japan (to T. M.). We thank Ms. Chikako Sakai and Mr. Hitoshi Moriuchi for their excellent technical assistance.

References

1. Ochs HD, Thrasher AJ. The Wiskott-Aldrich syndrome. J Allergy Clin Immunol. 2006;117:725–38.
2. Villa A, Notarangelo L, Macchi P, Mantuano E, Cavagni G, Brugnoni D, et al. X-linked thrombocytopenia and Wiskott-Aldrich syndrome are allelic diseases with mutations in the WASP gene. Nat Genet. 1995;9:414–7.
3. Imai K, Morio T, Zhu Y, Jin Y, Itoh S, Kajiwara M, et al. Clinicalcourse of patients with WASP gene mutations. Blood. 2004;103:456–64.
4. Albert MH, Bittner TC, Nonoyama S, Notarangelo LD, Burns S, Imai K, et al. X-linked thrombocytopenia (XLT) due to WAS mutations: clinical characteristics, long-term outcome, and treatment options. Blood. 2010;115:3231–8.
5. Dupuis-Girod S, Medioni J, Haddad E, Quartier P, Cavazzana-Calvo M, Le Deist F, et al. Autoimmunity in Wiskott-Aldrich syndrome: risk factors, clinical features, and outcome in a single-center cohort of 55 patients. Pediatrics. 2003;111:e622–7.
6. Boyd JK, Cheung CK, Molyneux K, Feehally J, Barratt J. An update on the pathogenesis and treatment of IgA nephropathy. Kidney Int. 2012;81:833–43.
7. Kawasaki Y. Mechanism of onset and exacerbation of chronic glomerulonephritis and its treatment. Pediatr Int. 2011;53:795–806.
8. Moldoveanu Z, Wyatt RJ, Lee JY, Tomana M, Julian BA, Mestecky J, et al. Patients with IgA nephropathy have increased serum galactose-deficient IgA1 levels. Kidney Int. 2007;71:1148–54.
9. Shimizu M, Nikolov NP, Ueno K, Ohta K, Siegel RM, Yachie A, et al. Development of IgA nephropathy-like glomerulonephritis associated with Wiskott-Aldrich syndrome protein deficiency. Clin Immunol. 2012;142:160–6.
10. Humblet-Baron S, Sather B, Anover S, Becker-Herman S, Kasprowicz DJ, Khim S, et al. Wiskott-Aldrich syndrome protein is required for regulatory T cell homeostasis. J Clin Invest. 2007;117:407–18.
11. Maillard MH, Cotta-de-Almeida V, Takeshima F, Nguyen DD, Michetti P, Nagler C, et al. The Wiskott-Aldrich syndrome protein is required for the function of $CD4^+CD25^+Foxp3^+$ regulatory T cells. J Exp Med. 2007;204:381–91.
12. Trifari S, Sitia G, Aiuti A, Scaramuzza S, Marangoni F, Guidotti LG, et al. Defective Th1 cytokine gene transcription in $CD4^+$ and $CD8^+$ T cells from Wiskott-Aldrich syndrome patients. J Immunol. 2006;177:7451–61.
13. Matsukura H, Kanegane H, Miya K, Ohtsubo K, Higuchi A, Tanizawa T, et al. IgA nephropathy associated with X-linked thrombocytopenia. Am J Kidney Dis. 2004;43:e7–12.
14. Shimizu M, Kanegane H, Wada T, Motoyoshi Y, Morio T, Candotti F, et al. Aberrant glycosylation of IgA in Wiskott-Aldrich syndrome and X-linked thrombocytopenia. J Allergy Clin Immunol. 2013;131:587–90.
15. Sakai O. IgA nephropathy: current concepts and future trends. Nephrology 1997;3: 2–3.
16. Imasawa T, Nagasawa R, Utsunomiya Y, Kawamura T, Zhong Y, Makita N, et al. Bone marrow transplantation attenuates murine IgA nephropathy: role of a stem cell disorder. Kidney Int. 1999;56:1809–17.
17. Suzuki H, Suzuki Y, Aizawa M, Yamanaka T, Kihara M, Pang H, et al. Th1 polarization in murine IgA nephropathy directed by bone marrow-derived cells. Kidney Int. 2007;72:319–27.
18. Inoue T, Sugiyama H, Kikumoto Y, Fukuoka N, Maeshima Y, Hattori H, et al. Downregulation of the beta1, 3- galactosyl transferasegene in tonsillar B lymphocytes and aberrant lectin bindings to tonsillar IgA as a pathogenesis of IgA nephropathy. Contrib Nephrol. 2007;157:120–4.
19. Yamada K, Kobayashi N, Ikeda T, Suzuki Y, Tsuge T, Horikoshi S, et al. Down-regulation of core 1 beta1, 3-galactosyl transferase and Cosmc by Th2 cytokine alters O-glycosylation of IgA1. Nephrol Dial Transplant. 2010;25:3890–7.

20. Suzuki H, Moldoveanu Z, Hall S, Brown R, Vu HL, Novak L, et al. IgA1-secreting cell lines from patients with IgA nephropathy produce aberrantly glycosylated IgA1. J Clin Invest. 2008;118: 629–39.
21. Suzuki H, Suzuki Y, Narita I, Aizawa M, Kihara M, Yamanaka T, et al. Toll-like receptor 9 affects severity of IgA nephropathy. J Am Soc Nephrol. 2008;19:2384–95.
22. Park HJ, Hahn WH, Suh JS, Kim MJ, Kang SW, Lee JS, et al. Association between toll-like receptor 10 (TLR10) gene polymorphisms and childhood IgA nephropathy. Eur J Pediatr. 2011;170: 503–9.
23. Kobayashi I, Nogaki F, Kusano H, Ono T, Miyawaki S, Yoshida H, et al. Interleukin-12 alters the physicochemical characteristics of serum and glomerular IgA and modifies glycosylation in a ddY mouse strain having high IgA levels. Nephrol Dial Transplant. 2002;17:2108–16.
24. Cuevas X, Lloveras J, Mir M, Aubia J, Masramon J. Disappearance of mesangial IgA deposits from the kidneys of two donors after transplantation. Transplant Proc. 1987;19:2208–9.
25. Koselj M, Rott T, Kandus A, Vizjak A, Malovrh M. Donor-transmitted IgA nephropathy: long-term follow-up of kidney donors and recipients. Transplant Proc. 1997;29:3406–7.
26. Ozsahin H, Cavazzana-Calvo M, Notarangelo LD, Schulz A, Thrasher AJ, Mazzolari E, et al. Long-term outcome following hematopoietic stem-cell transplantation in Wiskott-Aldrich syndrome: collaborative study of the European Society for Immunodeficiencies and European Group for Blood and Marrow Transplantation. Blood. 2008;111:439–45.

Identification of a novel erythroid-specific enhancer for the *ALAS2* gene and its loss-of-function mutation which is associated with congenital sideroblastic anemia

Kiriko Kaneko,[1,2] Kazumichi Furuyama,[1,6] Tohru Fujiwara,[3] Ryoji Kobayashi,[4] Hiroyuki Ishida,[5] Hideo Harigae,[3] and Shigeki Shibahara[1]

[1]Department of Molecular Biology and Applied Physiology, [2]Department of Endocrinology and Applied Medical Science, [3]Department of Hematology and Rheumatology, Tohoku University Graduate School of Medicine, Sendai, Miyagi; [4]Department of Pediatrics, Sapporo Hokuyu Hospital, Sapporo; [5]Department of Pediatrics, Kyoto Prefectural University of Medicine, Graduate School of Medical Science, Kyoto; and [6]Laboratory of Molecular Biochemistry, Iwate Medical University, Yahaba, Iwate, Japan

ABSTRACT

Erythroid-specific 5-aminolevulinate synthase (ALAS2) is the rate-limiting enzyme for heme biosynthesis in erythroid cells, and a missense mutation of the *ALAS2* gene is associated with congenital sideroblastic anemia. However, the gene responsible for this form of anemia remains unclear in about 40% of patients. Here, we identify a novel erythroid-specific enhancer of 130 base pairs in the first intron of the *ALAS2* gene. The newly identified enhancer contains a *cis*-acting element that is bound by the erythroid-specific transcription factor GATA1, as confirmed by chromatin immunoprecipitation analysis *in vivo* and by electrophoretic mobility shift assay *in vitro*. A promoter activity assay in K562 human erythroleukemia cells revealed that the presence of this 130-base pair region increased the promoter activity of the *ALAS2* gene by 10-15-fold. Importantly, two mutations, each of which disrupts the GATA-binding site in the enhancer, were identified in unrelated male patients with congenital sideroblastic anemia, and the lower expression level of ALAS2 mRNA in bone marrow erythroblasts was confirmed in one of these patients. Moreover, GATA1 failed to bind to each mutant sequence at the GATA-binding site, and each mutation abolished the enhancer function on ALAS2 promoter activity in K562 cells. Thus, a mutation at the GATA-binding site in this enhancer may cause congenital sideroblastic anemia. These results suggest that the newly identified intronic enhancer is essential for the expression of the *ALAS2* gene in erythroid cells. We propose that the 130-base pair enhancer region located in the first intron of the *ALAS2* gene should be examined in patients with congenital sideroblastic anemia in whom the gene responsible is unknown.

Introduction

The *ALAS2* gene encodes for erythroid-specific 5-aminolevulinate synthase (ALAS-E, EC 2.3.1.37), which is the rate-limiting enzyme of the heme biosynthetic pathway in erythroid cells.[1] It has been reported that the human *ALAS2* gene is mapped on the X chromosome,[2] and that a loss-of-function mutation of this gene causes X-linked sideroblastic anemia (XLSA),[3,4] which is the most common genetic form of congenital sideroblastic anemia (CSA). Moreover, a missense mutation of *ALAS2* was identified in a patient with non-familial CSA (nfCSA),[5] in which no family history of sideroblastic anemia was identified. In addition to *ALAS2*, several other genes were recently identified as causative genes for CSA, including *SLC25A38*,[6] *GLRX5*,[7] *ABCB7*,[8] *PUS1*,[9] and *SLC19A2*,[10] but the cause of sideroblastic anemia still remains undefined in more than 40% of patients with CSA.[11]

GATA1 transcription factor regulates the expression of several erythroid-specific genes, such as erythropoietin receptor gene,[12,13] α- and β-globin genes,[14,15] *ALAS2*[16] and the *GATA1* gene itself,[17] during erythroid differentiation.[18,19] Ablation of the *Gata1* gene in mice resulted in embryonic death because of anemia,[20] suggesting that GATA1 is essential for erythroid differentiation *in vivo*. It has been reported that GATA1 regulates transcription of human *ALAS2* through the proximal promoter region[16] and the erythroid-specific enhancer located in the eighth intron of *ALAS2*.[21] However, Fujiwara *et al.* demonstrated that the GATA1 protein binds to the *ALAS2* gene only in the middle of its first intron, where no regulatory region had so far been identified, by genome-wide analysis of K562 human erythroleukemia cells using chromatin immunoprecipitation followed by next-generation sequencing (ChIP-seq).[22]

In the present study, we have identified a novel erythroid-specific enhancer region in the first intron of the *ALAS2* gene. Moreover, we describe two mutations in the newly identified enhancer of *ALAS2*: a T-to-C transition, which changes GATA to GCTA at the GATA element in the antisense strand, in a pedigree with XLSA and one proband with nfCSA, and a 35-base pair (bp) deletion including the above-mentioned GATA element in a proband with nfCSA.

Methods

Polymerase chain reaction

DNA polymerases used for polymerase chain reaction (PCR) analysis were purchased from TAKARA BIO Inc. (Shiga, Japan). The

 doi:10.3324/haematol.2013.085449
The online version of this article has a Supplementary Appendix.
Manuscript received on February 4, 2013. Manuscript accepted on August 1, 2013.
Correspondence: furuyama@iwate-med.ac.jp

sequence of primers and probes used in this study are listed in the *Online Supplementary Tables*.

Polymerase chain reaction-based quantitative chromatin immunoprecipitation

Real-time PCR-based quantitative chromatin immunoprecipitation (ChIP-qPCR) analysis was conducted essentially as previously described.[22]

Electrophoretic mobility shift assay

Electrophoretic mobility shift assay (EMSA) was performed using "DIG Gel Shift Kit, 2nd Generation" (Roche Diagnostics GmbH, Mannheim, Germany), according to the manufacturer's protocol. Sequences of oligonucleotides for probes are indicated by the horizontal bar in the relevant figures. Nuclear extracts were prepared, as described previously,[23] from K562 cells or HEK293 human embryonic kidney cells that were transfected with a GATA1-FLAG fusion protein expression vector or its backbone vector.

Promoter/enhancer activity assays

Each target DNA fragment was prepared from genomic DNA from normal volunteers (WT) or patients with CSA (referred to as "GGTA" or "delGATA" in each reporter construct) and was cloned into pGL3basic plasmid (Promega Corporation, Madison, WI, USA). The human ALAS2 proximal promoter region (g.4820_5115, between -267 and +29 from the transcription start site)[16,24] was cloned into the multiple-cloning site of pGL3basic [referred to as pGL3-AEpro(-267)]. A single DNA fragment (5.2 kbp), carrying the ALAS2 proximal promoter, first exon, first intron and the untranslated region of the second exon, was subcloned into the multiple cloning site of pGL3basic [referred to as pGL3-AEpro(-267)+intron1]. A DNA fragment containing the GATA1-binding region in the first intron of the *ALAS2* gene (corresponding to g.7488_7960), which was defined by ChIP-seq analysis,[22] is referred to as the ChIP-peak. The length of the WT ChIP-peak is 473 bp. In addition, a 130-bp fragment containing ALAS2int1GATA, the consensus sequence for the GATA1-binding site in the ChIP-peak, is referred to as ChIPmini. Several deletion mutants of ChIPmini were prepared using pGL3-AEpro(-267)+ChIPmini(WT) as a template. The pGL3-TKpro plasmid was constructed by cloning herpes simplex virus thymidine kinase promoter into the multiple cloning site of pGL3basic plasmid. Each reporter vector and pEF-RL25 were introduced into K562 cells or HEK293 cells. Luciferase activity was determined using a dual-luciferase reporter system (Promega).

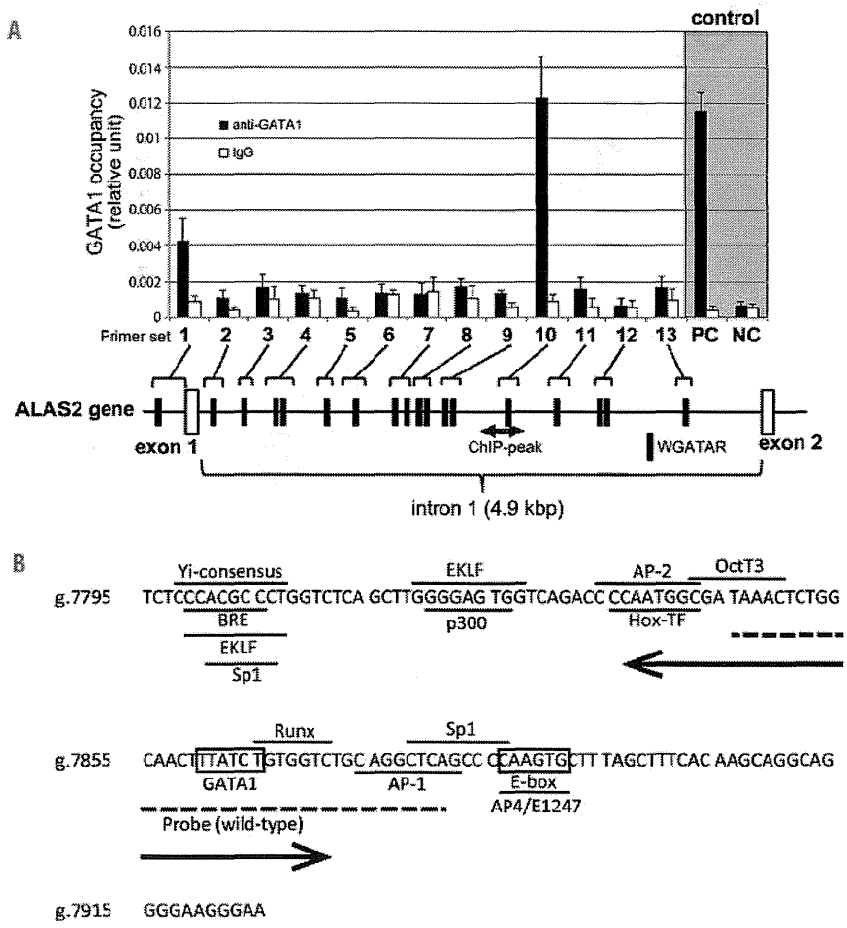

Figure 1. Identification of a functional GATA1 element in the first intron of the *ALAS2* gene. (A) Chromatin immunoprecipitation assay. Fragmented genomic DNA segments were immunoprecipitated with anti-GATA1 antibody or control IgG, and then precipitated fragments were quantified using real-time PCR as described in the *Online Supplementary Methods*. PC or NC indicates positive control or negative control, respectively, for the ChIP assay using anti-GATA1 in K562 cells.[22] One GATA element is present in the proximal promoter region and 17 GATA elements in the first intron (black symbols). The shaded double arrow indicates the region corresponding to ChIP-peak. (B) Nucleotide sequence of ChIPmini. The GATA binding site, ALAS2int1GATA, is located in the center of ChIPmini (boxed). A box also indicates the consensus for E-box that is bound by Scl/TAL1.[22] The sequence of ChIPmini was further analyzed for putative transcription factor binding sites using GeneQuest software (DNASTAR Inc., Madison, WI, USA), and the results are indicated by the horizontal bar. Yi-consensus, Yi transcription factor consensus site;[33] BRE, transcription factor IIB binding site;[34] EKLF, erythroid/Kruppel-like factor consensus site;[35] Sp1, stimulatory protein 1 binding site;[36] P300, P300 transcriptional coactivator consensus site;[37] AP-2, AP-2 beta consensus site;[38] Hox-TF, C1 element binding factor binding site;[39] OctT3, OctT3 binding site;[40] Runx, Runx proteins binding site;[41] AP-1, activator protein 1 binding site;[42] and AP4/E1247, AP4/E1247 binding site.[43] The sequence for the wild-type probe used in the EMSA is indicated by a dashed line. A double arrow indicates the deleted region of the delGATA mutation.

Identification of mutations of the ALAS2 gene

All exons including exon-intron boundaries, the proximal promoter region, and intron 1 and intron 8 of the *ALAS2* gene (GeneBank: NG_8983.1) were directly sequenced according to previously reported methods.[26]

Measurement of ALAS2 mRNA in purified erythroblasts

Total RNA was extracted from glycophorin A-positive bone marrow mononuclear cells, and was used for cDNA synthesis. ALAS2 expression was measured by real-time PCR, and was normalized to that of GAPDH mRNA.

Statistical analysis

Multiple comparisons between groups were made using the Tukey-Kramer test.

Patients

Eleven probands (eight pedigrees) with CSA of unknown cause were selected to determine the nucleotide sequence of the first intron of *ALAS2* gene. In these patients no disease-causative mutation was identified in the coding regions or reported regulatory regions in *ALAS2*, *SLC25A38*, *GLRX5*, *ABCB7*, *PUS1* and *SLC19A2*, which have been reported to be genes causing CSA[11] (see the *Online Supplementary Methods* for full details of the methods).

The genetic analyses performed in this project were approved by the ethical committee of Tohoku University School of Medicine. Blood samples were withdrawn from the probands and the family members after informed consent.

Results

Polymerase chain reaction-based quantitative chromatin immunoprecipitation analysis of the first intron of the ALAS2 gene

To identify the novel regulatory region for ALAS2 tran-

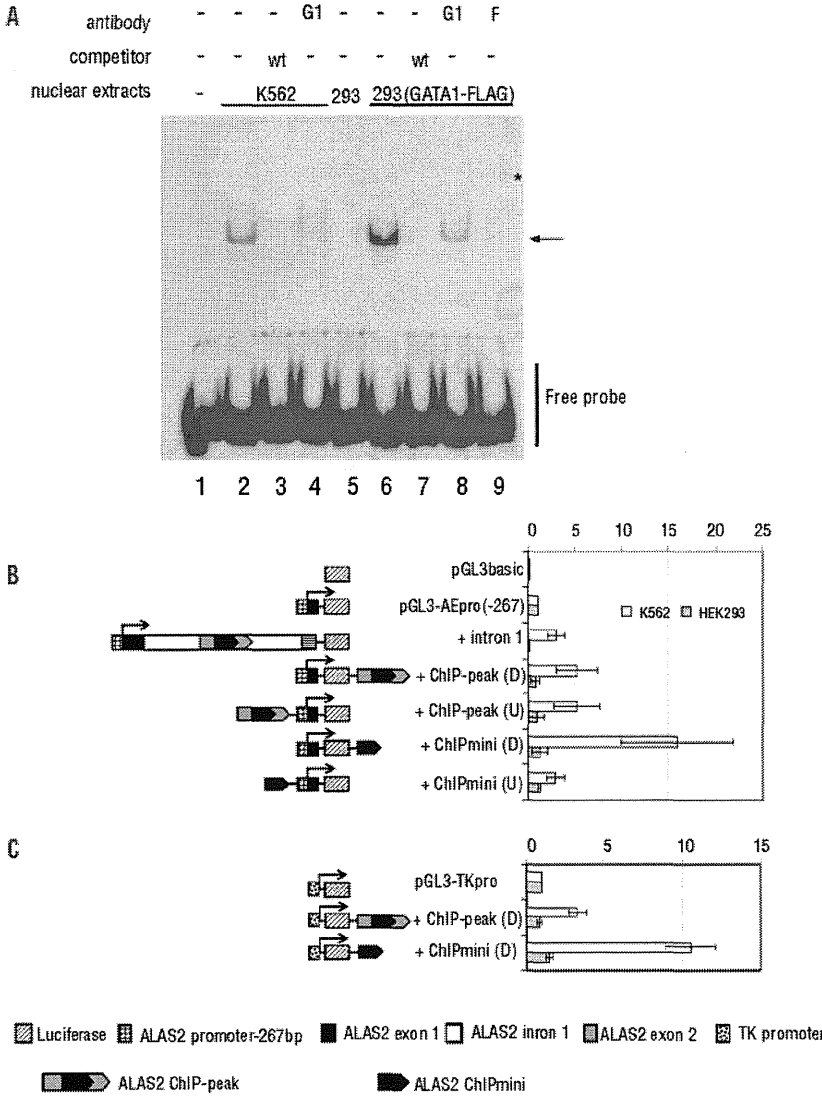

Figure 2. Functional analyses of ChIPmini present in the first intron of the *ALAS2* gene. (A) Electrophoretic mobility shift assay (EMSA). Wild-type (wt) probe was incubated with nuclear extracts prepared from K562 cells (lanes 2-4) or HEK293 cells expressing GATA1-FLAG (lanes 6-9). HEK293 cells were transfected with mock vector (lane 5) or FLAG-fused GATA1 expression vector before preparation of nuclear extracts. The protein-probe complex was detected as a retarded band (arrow). An excess amount of unlabeled probe (lanes 3, 7), anti-GATA1 antibody (G1) (lanes 4, 8) or anti-FLAG antibody (F) (lane 9) was included in the reaction mixture. Lane 1 shows the control without nuclear extracts. The asterisk indicates the super-shifted band (lane 9). (B) Functional analysis of ChIPmini as an enhancer for the *ALAS2* gene. Details of the fragments for each plasmid, such as intron1, ChIP-peak and ChIPmini, are described in the *Methods* section. Each DNA fragment was inserted upstream of the *ALAS2* proximal promoter or downstream of luciferase cDNA, indicated as (U) or (D), respectively. Results are expressed as a relative activity compared to that of pGL3-AEpro(-267), and are presented as the mean ± standard deviation (SD) of three independent experiments. (C) Functional analysis of ChIPmini as an enhancer for non-erythroid gene promoter. The enhancer activity of the first intron was examined using the herpes simplex virus TK promoter as a non-erythroid promoter. ChIP-peak or ChIPmini was inserted downstream of the luciferase gene of pGL3-TKpro, yielding pGL3-TKpro+ChIP-peak(D) or pGL3-TKpro+ChIPmini(D). Each of these reporter vectors was introduced into K562 cells or HEK293 cells to measure enhancer activity. Results are expressed as a relative activity compared to that of pGL3-TKpro, and are presented as the mean ± SD of three independent experiments.

scription, we first performed ChIP-qPCR analysis in K562 cells to localize the GATA1-binding region of the *ALAS2* gene *in vivo*, which was determined by genome-wide ChIP-seq analysis.[22] In fact, ChIP-qPCR enabled us to examine the GATA1-binding activity of an individual GATA element or two adjacent GATA elements in the first intron of the *ALAS2* gene. Based on a search of NCBI Reference Sequence (NG_8983.1) using SeqBuilder software (DNASTAR Inc., Madison, WI, USA), we identified 17 GATA elements (16 out of 17 GATA elements are present in the antisense orientation) in the first intron of human *ALAS2* (Figure 1A), which is compatible with the previous report.[21] We also included the proximal promoter region that contains a functional GATA-binding site (g.4961_4966).[16] Overall 13 primer sets were designed to amplify the GATA elements located in the proximal promoter region and the first intron of *ALAS2* (Figure 1A and *Online Supplementary Table S1*). Among the 12 primer sets targeting the first intron, using primer set 10, we could amplify genomic DNA that was precipitated with anti-GATA1 antibody at a similar level to that of the positive control, but not with other primer sets. We refer to this region amplified with primer set 10 as ChIPmini (g.7795_7924), the sequence of which is shown in Figure 1B. *In silico* analysis identified only one GATA element (g.7860_7865, boxed in Figure 1B) in ChIPmini, termed ALAS2int1GATA. In addition, primer set 1 which targets the proximal promoter region yielded notable amounts of amplified genome DNA. These results indicate that GATA1 protein bound to the regions amplified with primer sets 1 and 10 in K562 cells; that is, GATA1 protein could bind to the proximal promoter region as well as to ALAS2int1GATA in the first intron of the *ALAS2* gene *in vivo*. Since the GATA element located in the proximal promoter has been well examined *in vitro*,[16] we further determined the functional features of ALAS2int1GATA.

GATA1 protein binds to ALAS2int1GATA located in ChIPmini

We then examined whether GATA1 protein binds to ALAS2int1GATA present in the center of ChIPmini using EMSA (Figure 2A). The WT probe contains ALAS2int1GATA (Figure 1B). The incubation of labeled WT probe with nuclear extracts of K562 cells yielded the retarded band that represents the protein-probe complex (lane 2), whereas this retarded band was undetectable with an excess amount of non-labeled WT probe (lane 3). Moreover, the addition of anti-GATA1 antibody reduced the intensity of the retarded band (lane 4), suggesting that GATA1 protein may bind to the WT probe. In fact, the retarded band was not detected when the labeled probe was incubated with nuclear extracts of mock-transfected HEK293 cells (lane 5). In contrast, the retarded band was observed when the labeled probe was incubated with the nuclear extracts of HEK293 cells expressing FLAG-fused GATA1 (lane 6). Importantly, the retarded band observed in lane 6 was not detectable in the presence of an excess amount of non-labeled probe (lane 7). The formation of the retarded band was partially inhibited by anti-GATA1 antibody (lane 8). Likewise, the inclusion of anti-FLAG antibody (lane 9) resulted in the disappearance of the retarded band and instead generated the super-shifted band (indicated by an asterisk). These results suggest that GATA1 protein binds to the WT probe containing ALAS2int1GATA.

Enhancement of ALAS2 promoter activity by the DNA segment containing ALAS2int1GATA

To examine the functional importance of ALAS2int1GATA in the promoter activity of the *ALAS2* gene (Figure 2B), we constructed the pGL3-AEpro(-267) vector, in which the expression of firefly luciferase gene is controlled under the proximal promoter of the *ALAS2* gene (g.4820_5115). The presence of the first intron of *ALAS2* (pGL3-AEpro(-267)+intron1) increased luciferase activity about 3-fold in K562 cells, whereas luciferase activity was decreased to 10% of pGL3-AEpro(-267) in HEK293 cells. When the ChIP-peak, the region determined by ChIP-seq analysis (g.7488_7960),[22] was present downstream [+ChIP-peak(D)] or upstream [+ChIP-peak(U)] of the ALAS2 proximal promoter, luciferase activity was increased about 5-fold, irrespective of the location, compared to that of pGL3-AEpro(-267) in K562 cells. Moreover, the presence of the ChIPmini fragment downstream of the luciferase gene [+ChIPmini (D)] resulted in a 16-fold increase of luciferase activity. However, when the same fragment was inserted upstream of the ALAS2 promoter [+ChIPmini(U)], luciferase activity increased only 3-fold. Thus, the enhancer activity of the ChIPmini fragment varies, depending on its location. Moreover, among the constructs examined, the ChIPmini fragment showed maximum enhancer activity downstream of the luciferase gene. The ChIP-peak or ChIPmini fragment downstream of the ALAS2 promoter influenced luciferase activity marginally (0.73- or 1.25-fold, respectively) in HEK293 cells (Figure 2B). These results suggest that the enhancer activity of each fragment containing ALAS2int1GATA is specific to erythroid cells.

To examine whether the erythroid-specific enhancer activity depends on the ALAS2 promoter, we replaced the ALAS2 promoter with the herpes simplex virus TK promoter (Figure 2C). The ChIP-peak and ChIPmini enhanced TK promoter activity 3.4- and 9.8-fold in K562 cells, respectively, whereas they did not enhance TK promoter activity in HEK293 cells. These results indicate that the erythroid-specific enhancer is present in the ChIP-peak and ChIPmini fragments. In addition, the erythroid-specific enhancer is functional in the non-erythroid gene promoter.

Identification of mutations in the first intron of the ALAS2 gene in patients with congenital sideroblastic anemia

Considering the newly identified enhancer in the first intron of the *ALAS2* gene, we examined whether some CSA patients carry the mutation in ChIP-peak or ChIPmini of *ALAS2*. We determined the nucleotide sequence of the first intron of *ALAS2* in 11 probands (eight pedigrees), and found two distinct mutations in the newly identified enhancer region in five Japanese patients (three pedigrees). The clinical features and hematologic status of the probands at diagnosis of the disease are summarized in Table 1.

Proband 1 in a pedigree with XLSA

The first male Japanese proband was referred to hospital at the age of 3 months to investigate the cause of his pale face. No problems were reported during the birth. Investigations showed microcytic/hypochromic anemia, an increased concentration of serum iron and raised serum ferritin level. Bone marrow aspiration revealed the presence of ring sideroblasts. Two maternal relatives – male cousins of the proband's mother – have sideroblastic ane-

mia (Figure 3A). The pedigree of this family suggested X chromosome-linked inheritance of the disease. The proband's anemia was not improved by pyridoxine administration (5 mg/kg/day for 3 months), and the boy required once monthly transfusions of one unit of concentrated red blood cells to maintain an adequate hemoglobin level. At the age of 7 months, this proband died of sepsis caused by alpha-streptococcus.

Proband 2 with nfCSA

The second male Japanese proband visited hospital at the age of 4 years because of the paleness of his complexion. Investigations showed microcytic/hypochromic anemia, mild thrombocytosis, and a high serum iron concentration with a normal serum ferritin concentration. Bone marrow aspiration revealed the presence of ring sideroblasts (38% of the erythroblasts). Giant platelets were observed in the bone marrow, although dysplasia of the megakaryocytes was not clear. There was no family history of sideroblastic anemia (Figure 3B).

Proband 3 with nfCSA

The third male Japanese proband was noted to have anemia at the age of 2 years, but details are not available. Without any treatment, serum hemoglobin level was maintained at 70 g/L, and increased to 100 g/L at the age of 10. Accordingly, the proband stopped visiting the hospital. At the age of 19, however, the proband was admitted to hospital because of general fatigue. Investigations revealed microcytic, hypochromic anemia with systemic iron overload. The presence of ring sideroblasts was confirmed in his bone marrow by Prussian blue staining (36% of erythroblasts). Although this proband was treated with pyridoxine (150 mg/day) for 8 months, his anemia did not improve. There was no family history of sideroblastic anemia (Figure 3C).

In proband 1 from the pedigree with XLSA (Figure 3A), we identified a single nucleotide mutation (Figure 4, upper panel, g.7863T>C), which alters the core sequence of ALAS2int1GATA in the antisense strand from GATA to GGTA (referred to as "GGTA mutation"). The same mutation of the *ALAS2* gene was also identified in two cousins of the proband's mother, both of whom were diagnosed as having sideroblastic anemia (Figure 3A). Clinical specimens for genetic analysis were not available from either the parents or the elder brother of proband 1.

The same GGTA mutation was identified at ALAS2int1GATA in proband 2 with CSA (Figure 4, middle panel). There was no known consanguinity between proband 1 and proband 2. Genomic DNA from the parents of proband 2 was not available, because they did not agree to provide their clinical specimens for genetic analysis. Since proband 2 was also noted to have thrombocytosis (Table 1), we searched for a *JAK2* mutation in the genomic DNA extracted from the peripheral blood of this patient. However, no V617F mutation or any missense

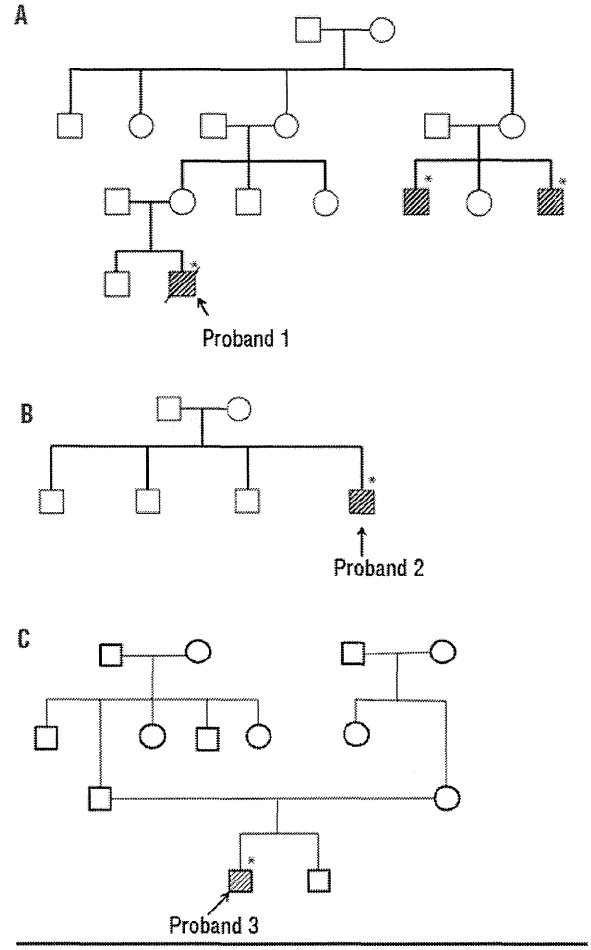

Figure 3. Family trees of three unrelated probands. Family tree of: (A) proband 1 with XLSA, (B) proband 2 with nfCSA, and (C) proband 3 with nfCSA. Shaded boxes indicate affected individuals in each pedigree. Asterisks indicate the individuals in whom a mutation in the first intron of the *ALAS2* gene was detected.

Table 1. **Hematologic status of each proband at diagnosis of the disease.**

	Onset of the anemia	Age at diagnosis of SA	Family history of XLSA	Hb (g/L)	MCV (fL)	MCH (pg)	Platelets (x10⁹/L)	Serum iron (μmol/L)	Ferritin (pmol/L)
Proband 1	4 months	4 months	yes	39 [136-183]	65 [83-101]	18.7 [28-35]	246 [140-379]	63.9 [10.7-37.6]	399.7 [49.4-270]
Proband 2	4 years	4 years	no	84 [126-165]	73.4 [87-104]	22 [29-35]	610 [138-309]	49.1 [12.5-25.0]	670.1 [67.4-725]
Proband 3	2 years	19 years	no	78 [120-165]	73.9 [80-100]	22.2 [28-34]	373 [160-420]	39.6 [14.3-21.5]	2489.7 [40.4-288]

The normal value of each clinical examination is shown in brackets. SA: sideroblastic anemia; XLSA: X-linked sideroblastic anemia; Hb: hemoglobin; MCV: mean corpuscular volume; MCH: mean corpuscular hemoglobin.

mutation in exon 12, each of which is frequently observed in patients with refractory anemia with ring sideroblasts and thrombocytosis (RARS-T),[27] was detected (*data not shown*). Thus, the GGTA mutation at ALAS2int1GATA may be responsible for the sideroblastic anemia in proband 2.

In proband 3 with CSA, a deletion of 35 bp was identified in the first intron of the *ALAS2* gene (Figure 4A, lower panel, g.7836_7870del, referred to as "delGATA mutation"). The delGATA mutation results in the loss of ALAS2int1GATA. However, the delGATA mutation was not identified in the *ALAS2* gene of the parents of proband 3 (*data not shown*). Thus, the delGATA mutation may be a *de novo* mutation or a somatic mutation. Accordingly, we compared the relative ALAS2 mRNA level in the erythroid progenitor cells isolated from proband's bone marrow with those of normal subjects. The ALAS2 mRNA level was more than 7-fold lower in the proband's erythroblasts than in those of three independent, normal subjects (Figure 4B), suggesting that the delGATA mutation may lead to decreased transcription of the *ALAS2* gene.

Lastly, we examined the sequence of the region corresponding to g.7513_8165 of the *ALAS2* gene, which contains ChIPmini, in 103 healthy, Japanese volunteers (44 males and 59 females, total 162 alleles) using PCR followed by direct sequencing. No mutation was found in this region (*data not shown*). In addition, no single nucleotide polymorphism was reported in this GATA element, based on the single nucleotide polymorphism database available at the NCBI home page (*http://www.ncbi.nlm.nih.gov/snp*, current assembly is GRCh37.p5). Thus, the GGTA mutation and delGATA mutation at ALAS2int1GATA may be unique to patients with sideroblastic anemia. Taken together, we suggest that the newly identified mutations at ALAS2int1GATA are responsible for sideroblastic anemia.

The mutation at ALAS2int1GATA impairs GATA1-binding activity and enhancer function

We examined the effect of the GGTA mutation or the delGATA mutation on the binding of GATA1 protein to ALAS2int1GATA using each mutant probe (Figure 5A). The delGATA probe represents the 5'- and 3'-flanking sequences of the deleted 35-bp segment (see Figure 4A). As shown in Figure 5B, the incubation of labeled WT probe with nuclear extracts from HEK293 cells expressing FLAG-fused GATA1

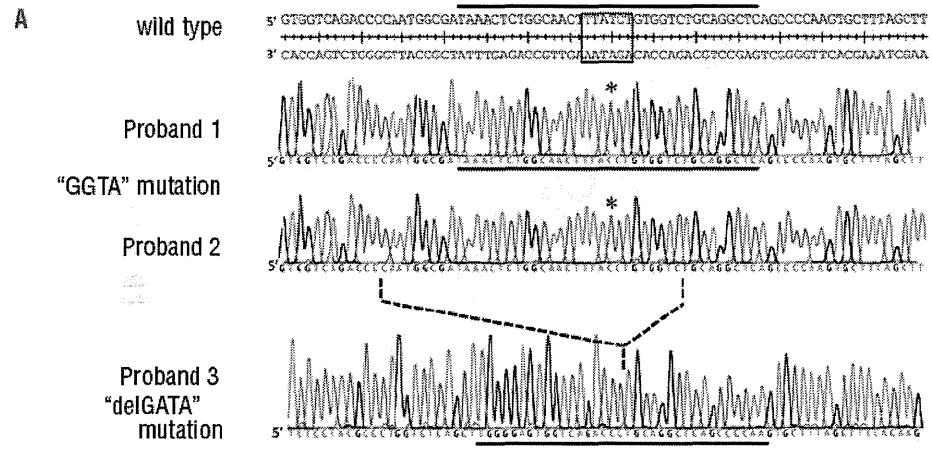

Figure 4. Identification of mutations in the first intron of the *ALAS2* gene in a patient with XLSA and two patients with nfCSA. (A) *ALAS2* mutations in three probands. Upper, middle and lower panels show the sequences of the flanking regions of ALAS2int1GATA (boxed in the wild-type sequence) in the *ALAS2* gene of probands 1, 2 and 3, respectively. Asterisks indicate the T to C transition in the sense strand identified in the *ALAS2* gene of proband 1 and proband 2 with CSA. The broken line between the middle and lower panels indicates the deleted region identified in proband 3 with CSA. The solid horizontal bar in each panel indicates the sequence of the sense strand of each probe used for the EMSA (see Figures 3A and 5B). (B) ALAS2 mRNA expression in erythroblasts of proband 3. ALAS2 mRNA levels were determined in purified erythroblasts isolated from proband 3 and three independent normal individuals using real-time PCR. Results are expressed as the mean ± SD of three independent experiments.

showed a retarded band (lane 3): this band was super-shifted by the addition of anti-FLAG antibody (lane 4), or undetectable with non-labeled WT probe (lane 5), whereas the non-labeled GGTA probe (lane 6) or delGATA probe (lane 7) could not compete for the labeled WT probe. Furthermore, the retarded band was not detectable when labeled GGTA probe (lane 8) or delGATA probe (lane 9) was incubated with the nuclear extracts of HEK293 cells expressing FLAG-fused GATA1. These results suggest that either the GGTA mutation or the delGATA mutation may impair the binding of GATA1 to ALAS2int1GATA.

We then examined the influence of the point mutation or deletion of ALAS2int1GATA on the enhancing activity of the first intron of the *ALAS2* gene (Figure 6A). The GGTA mutation decreased the enhancing activity of the first intron, ChIP-peak or ChIPmini in K562 cells to 17.0%, 18.5% or 12.9%, respectively, of that of the WT construct. The delGATA mutation decreased the enhancing activity of the first intron of *ALAS2*, ChIP-peak or ChIPmini in K562 cells to 10.5%, 15.7% or 12.6%, respectively, of that of the WT construct. In contrast, the relative luciferase activity of the construct carrying each mutation was only marginally different from that of WT intron 1, ChIP-peak or ChIPmini in HEK293 cells (Figure 6A), thereby confirming that ALAS2int1GATA functions as an erythroid-specific enhancer.

There are several potential *cis*-elements at the flanking regions of ALAS2int1GATA, such as EKLF and Sp1, each of which may be involved in the erythroid-specific transcriptional regulation of the *ALAS2* gene.[16,21] We thus analyzed the roles of these *cis*-elements in the enhancer activity of ALAS2int1GATA using deletion mutants at the 5'- or 3'-flanking region of ChIPmini, constructed in pGL3-AEpro(-267)+ChIPmini(D). Deletion of the EKLF1 element at the 5'-flanking region or both E-box and Sp1 elements at the 3'-flanking region did not significantly influence the enhancer activity of ChIPmini (Figure 6B). It should be noted that the Sp1 site overlaps with the 3'-portion of the AP-1 site and the 5'-portion of the E-box (Figure 6C). Moreover, deletion at the 5'-flanking region of ChIPmini ("delEKLF2", "delAP2" and "delOctT3") marginally decreased the enhancer activity (Figure 6B), but the change was not statistically significant. In contrast, deletion of the AP-1 element at the 3'-flanking region ("delAP1" in Figure 6B) significantly decreased the enhancer activity, by about 40% of the activity of ChIPmini(WT). The significant decrease of enhancer activity was observed only in ChIPmini(GGTA), ChIPmini(delGATA) and delAP1, compared to the activity of ChIPmini(WT) (*P<0.05 and **P<0.01 in Figure 6B). We next constructed another reporter vector that carries an internal deletion of the 5' portion of the AP-1 element with an intact Sp1 site ("lackAP1" in Figure 6B). Internal deletion of the AP-1 element alone in ChIPmini decreased the enhancer activity, although not to a statistically significant degree. Thus, the entire AP-1 element seems to be important for the

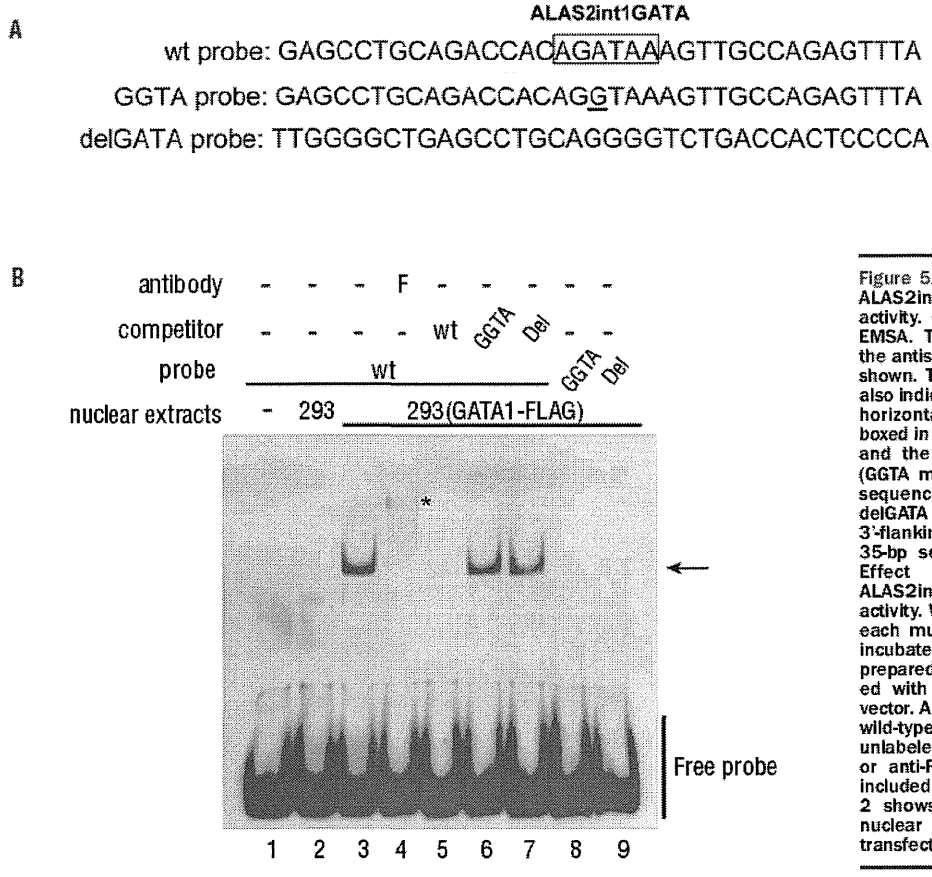

Figure 5. Effects of the mutations of ALAS2int1GATA on GATA1-binding activity. (A) DNA probes used in the EMSA. The nucleotide sequences in the antisense strand of the probes are shown. The position of each probe is also indicated in Figure 1B as the solid horizontal bar. ALAS2int1GATA is boxed in the sequence of the wt probe, and the single nucleotide transition (GGTA mutation) is underlined in the sequence of the GGTA probe. The delGATA probe represents the 5'- and 3'-flanking sequences of the deleted 35-bp segment (see Figure 3B). (B) Effect of each mutation of ALAS2int1GATA on GATA1-binding activity. Wild-type probe (lanes 3-7) or each mutant probe (lanes 8, 9) was incubated with the nuclear extracts prepared from HEK293 cells transfected with the GATA1-FLAG expression vector. An excess amount of unlabeled wild-type probe (lane 5), each of the unlabeled mutant probes (lanes 6, 7), or anti-FLAG antibody (lane 4) was included in the reaction mixture. Lane 2 shows the negative control with nuclear extracts from HEK293 cells transfected with mock vector.

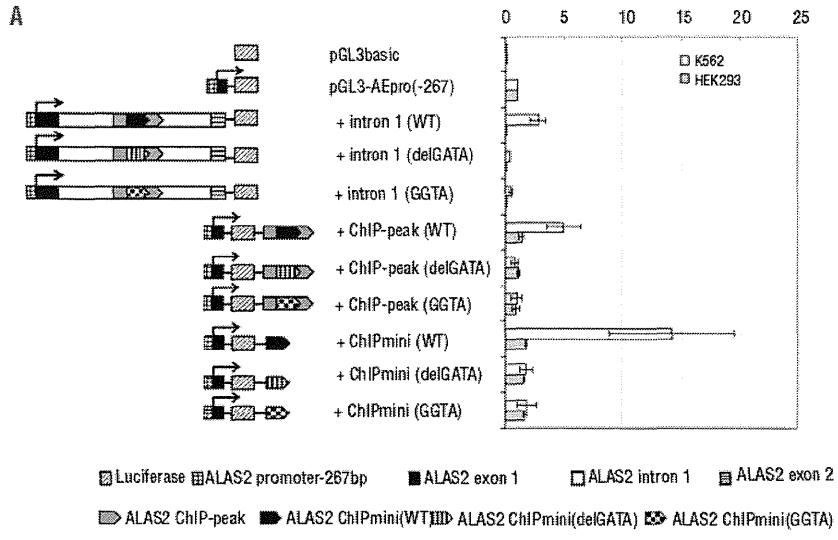

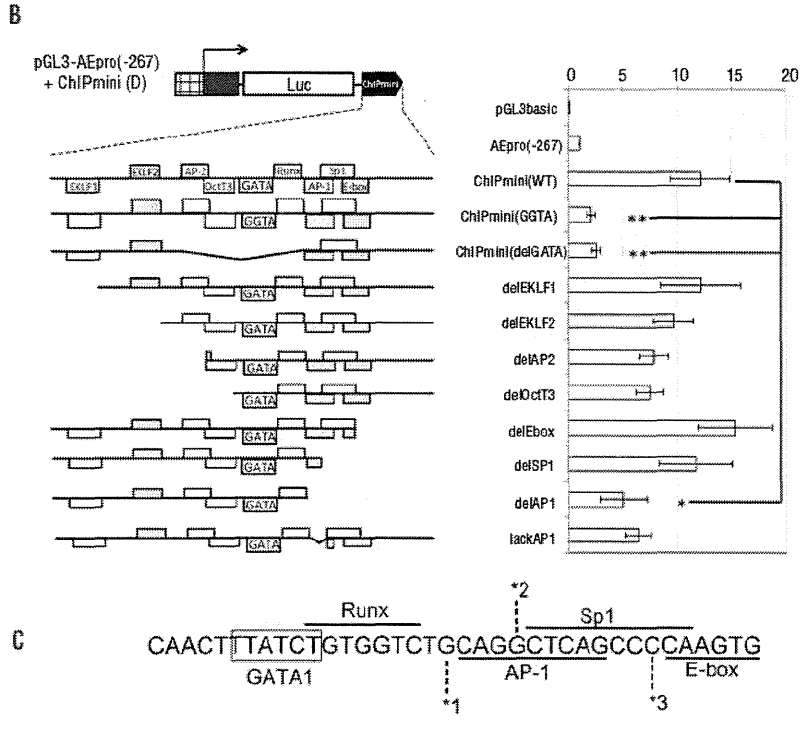

Figure 6. Identification of *cis*-elements essential for the erythroid-specific enhancer activity of ChIPmini. (A) Effect of each mutation of ALAS2int1GATA on the enhancer activity of *ALAS2* ChIPmini. The region corresponding to +intron1, ChIP-peak or ChIPmini, derived from proband 1 or proband 3, was subcloned into pGL3-AEpro(-267) to construct the reporter vector containing the GGTA mutation or the deletion of ALAS2int1GATA, respectively. (B) Effect of the deletion at the 5'- or 3'-flanking region of ALAS2int1GATA on the enhancer activity of ChIPmini. The 5'- and 3'-flanking regions of ALAS2int1GATA contain potential transcription factor-binding sites (*cis*-elements), and a portion of each flanking region was deleted, as schematically shown. The enhancer activity of each deletion mutant was determined in K562 erythroleukemia cells. (C) The nucleotide sequence of the 3'-flanking region of ALAS2int1GATA. Note that the Sp1 site overlaps the AP-1 site and E-box. Each number, *1, *2 or *3, indicates the nucleotide at the 3' end of the deletion mutant, delAP1, delSP1 or delE-box, respectively. Thus, delSP1 also lacks the 3' portion of the AP-1 site. (D) Effect of deletion of the 5'- and 3'-flanking regions of ALAS2int1GATA on the enhancer activity of ChIPmini. The construct, delEKLF2/delSP1, lacks two EKLF sites in the 5'-flanking region and both the Sp1 element and E-box in the 3'-flanking region. The AP-1 element at the 3'-flanking region was deleted from delEKLF2/delSP1, yielding delEKLF2/delAP1. Results are expressed as relative activity compared to that of pGL3-AEpro(-267), and are presented as the mean ± SD of at least three independent experiments.

enhancer activity of ChIPmini (WT) (Figure 6B).

Consequently, we constructed delEKLF2/delSP1 and delELKLF2/delAP1, each of which lacks EKLF elements at the 5'-flanking region and the Sp1 element or the AP-1 element at the 3'-flanking region, respectively (Figure 6D). The deletion mutant, delEKLF2/delSP1, still retained enhancer activity at about 80% of that of ChIPmini(WT), whereas delEKLF2/delAP1 showed decreased enhancer activity similar to the activity of ChIPmini(GGTA). These data indicate that ALAS2int1GATA and its flanking region, especially the AP-1 element, are critically important for the erythroid-specific enhancer activity of ChIPmini.

Taken together, these results suggest that the ChIPmini region acts as an erythroid-specific enhancer for the *ALAS2* promoter, and that both the GGTA mutation and the delGATA mutation represent loss-of-function mutations of ALAS2int1GATA.

Discussion

In the present study, we identified an erythroid-specific enhancer region in the first intron of the human *ALAS2* gene (a 130 bp region referred to as ChIPmini), a region which contains ALAS2int1GATA, a functional GATA1-binding site. We also identified the GGTA mutation and the delGATA mutation at ALAS2int1GATA, each of which is associated with XLSA or CSA. Moreover, we confirmed that each mutation diminished the binding of GATA1 transcription factor to ALAS2int1 (Figure 5B) and decreased enhancer activity of ChIPmini (Figure 6A). Thus, the GGTA mutation and delGATA mutation are loss-of function mutations of the *ALAS2* gene. In fact, the expression of ALAS2 mRNA in bone marrow erythroblasts was lower in proband 3 (Figure 4B) than in normal controls. Thus, each loss-of function mutation may lead to decreased transcription of the *ALAS2* gene, thereby causing sideroblastic anemia in male patients. Such a molecular basis is consistent in part with the lack of pyridoxine responsiveness in these patients (see "Patients" section).

The intronic enhancer, ChIPmini, increased ALAS2 promoter activity most efficiently in erythroid cells when it was present downstream of the promoter (Figure 2B). ChIPmini contains potential *cis*-acting elements, including two EKLF-binding sites, each of which overlaps with the Sp1-binding site or p300-binding site, AP-2 site, OctT3 site Runx site, AP-1 binding site, Sp1 site, and E-box (Figure 1B). Further analysis using deletion mutants of ChIPmini revealed that the potential AP-1 binding site at the 3'-flanking region might be involved in the erythroid-specific enhancer activity of ChIPmini (Figure 6B). These results suggest that ALAS2int1GATA and its 3'-flanking region are essential for the erythroid-specific enhancer activity of ChIPmini. In fact, EKLF[26] and AP-1[29] are involved in erythroid-specific gene expression. It is interesting that the inclusion of the whole first intron of the *ALAS2* gene in a reporter construct resulted in a decrease of ALAS2 promoter activity [11% of pGL3-AEpro(-267)] in non-erythroid HEK293 cells (Figures 2B and 6A). Likewise, the ChIP-peak upstream or downstream of the promoter also reduced the promoter activity in HEK293 cells [73% or 88% of pGL3-AEpro(-267), respectively] (Figure 2B). These results suggest that the first intron of the *ALAS2* gene may contain suppressor element(s) in addition to the erythroid-specific enhancer, although the mechanism of the suppression and the relevant region remain elusive.

We have successfully identified a novel erythroid-specific enhancer for ALAS2 expression, and have identified disease-causative mutations of this enhancer in patients with CSA. Despite the fact that about 50 missense or non-sense mutations of the *ALAS2* gene have been reported as disease-causative mutations in patients with XLSA,[3,30] a mutation in the regulatory region for the transcription of *ALAS2* has rarely been reported to date. Ducamp *et al.* reported a 48-bp deletion of the *ALAS2* gene at the proximal promoter region (c.-91_-44del) in a patient with XLSA, and proposed that the identified deletion would cause XLSA, since the level of ALAS2 mRNA in the proband's bone marrow was lower than that of normal controls.[31] In this context, it has been reported that the deleted region contained a functionally important element for ALAS2 transcription.[16] Bekri *et al.* reported a C-to-G transversion at nucleotide -206 (c.-258C>G) from the transcription start site in the proximal region of the human *ALAS2* gene in patients with XLSA;[24] however, May *et al.* identified this transversion in normal individuals from South Wales at the rate of 0.05, suggesting that this promoter mutation is a polymorphism.[32]

In conclusion, we have identified a novel erythroid-specific enhancer in the first intron of the human *ALAS2* gene, the enhancer function of which may be directed by GATA1 with other transcription factors, such as EKLF and AP-1 binding proteins. Furthermore, we identified the loss-of-function mutation of ALAS2int1GATA, the GATA element within this enhancer, in five of 11 patients with CSA in whom the gene responsible could not be identified. Thus, the intronic region containing ALAS2int1GATA of the *ALAS2* gene should be examined in patients with XLSA or nfCSA in whom the genetic mutation causing the sideroblastic anemia is unknown.

Acknowledgments

This work was supported in part by a Grant-in-Aid for Scientific Research (C) (to KF) and Health and Labour Sciences Research Grants (to HH and KF). The authors thank Prof. Norio Komatsu (Juntendo University) for examination for the JAK2 mutation. We are also grateful to the Biomedical Research Core of Tohoku University Graduate School of Medicine for allowing us to use various facilities.

Authorship and Disclosures

Information on authorship, contributions, and financial & other disclosures was provided by the authors and is available with the online version of this article at www.haematologica.org.

References

1. Anderson KE, Sassa S, Bishop DF, Desnick RJ. Disorders of heme biosynthesis: X-linked sideroblastic anemia and the porphyrias. In: Scriver CR, Beaudet AL, Sly WS, Valle D, eds. The Metabolic & Molecular Bases of Inherited Disease. New York: McGraw-Hill Medical Publishing Division, 2001:2991-3062.
2. Cotter PD, Willard HF, Gorski JL, Bishop DF. Assignment of human erythroid delta-aminolevulinate synthase (ALAS2) to a distal subregion of band Xp11.21 by PCR analysis of somatic cell hybrids containing X; autosome translocations. Genomics. 1992;13(1):211-2.

3. Bottomley SS. Sideroblastic Anemias. In: Greer JP, Foerster J, Rogers GM, Paraskevas F, Glader B, Arber DA, et al., eds. Wintrobe's clinical hematology. 12th ed. Philadelphia I London: Wolters Kluwer Health/Lippincott Williams & Wilkins, 2009:835-56.
4. Ohba R, Furuyama K, Yoshida K, Fujiwara T, Fukuhara N, Onishi Y, et al. Clinical and genetic characteristics of congenital sideroblastic anemia: comparison with myelodysplastic syndrome with ring sideroblast (MDS-RS). Ann Hematol. 2013;92(1):1-9.
5. Harigae H, Furuyama K, Kudo K, Hayashi N, Yamamoto M, Sassa S, et al. A novel mutation of the erythroid-specific gamma-aminolevulinate synthase gene in a patient with non-inherited pyridoxine-responsive sideroblastic anemia. Am J Hematol. 1999;62(2):112-4.
6. Guernsey DL, Jiang H, Campagna DR, Evans SC, Ferguson M, Kellogg MD, et al. Mutations in mitochondrial carrier family gene SLC25A38 cause nonsyndromic autosomal recessive congenital sideroblastic anemia. Nat Genet. 2009;41(6):651-3.
7. Camaschella C, Campanella A, De Falco L, Boschetto L, Merlini R, Silvestri L, et al. The human counterpart of zebrafish shiraz shows sideroblastic-like microcytic anemia and iron overload. Blood. 2007;110(4):1353-8.
8. Allikmets R, Raskind WH, Hutchinson A, Schueck ND, Dean M, Koeller DM. Mutation of a putative mitochondrial iron transporter gene (ABC7) in X-linked sideroblastic anemia and ataxia (XLSA/A). Hum Mol Genet. 1999;8(5):743-9.
9. Bykhovskaya Y, Casas K, Mengesha E, Inbal A, Fischel-Ghodsian N. Missense mutation in pseudouridine synthase 1 (PUS1) causes mitochondrial myopathy and sideroblastic anemia (MLASA). Am J Hum Genet. 2004; 74(6):1303-8.
10. Labay V, Raz T, Baron D, Mandel H, Williams H, Barrett T, et al. Mutations in SLC19A2 cause thiamine-responsive megaloblastic anaemia associated with diabetes mellitus and deafness. Nat Genet. 1999;22 (3):300-4.
11. Bergmann AK, Campagna DR, McLoughlin EM, Agarwal S, Fleming MD, Bottomley SS, et al. Systematic molecular genetic analysis of congenital sideroblastic anemia: evidence for genetic heterogeneity and identification of novel mutations. Pediatr Blood Cancer. 2010;54(2):273-8.
12. Zon LI, Youssoufian H, Mather C, Lodish HF, Orkin SH. Activation of the erythropoietin receptor promoter by transcription factor GATA-1. Proc Natl Acad Sci USA. 1991; 88(23):10638-41.
13. Chiba T, Ikawa Y, Todokoro K. GATA-1 transactivates erythropoietin receptor gene, and erythropoietin receptor-mediated signals enhance GATA-1 gene expression. Nucleic Acids Res. 1991;19(14):3843-8.
14. Evans T, Felsenfeld G. The erythroid-specific transcription factor eryf1: a new finger protein. Cell. 1989;58(5):877-85.
15. Whitelaw E, Tsai SF, Hogben P, Orkin SH. Regulated expression of globin chains and the erythroid transcription factor GATA-1 during erythropoiesis in the developing mouse. Mol Cell Biol. 1990;10(12):6596-606.
16. Surinya KH, Cox TC, May BK. Transcriptional regulation of the human erythroid 5-aminolevulinate synthase gene. Identification of promoter elements and role of regulatory proteins. J Biol Chem. 1997;272(42):26585-94.
17. Kobayashi M, Nishikawa K, Yamamoto M. Hematopoietic regulatory domain of gata1 gene is positively regulated by GATA1 protein in zebrafish embryos. Development. 2001;128(12):2341-50.
18. Ohneda K, Yamamoto M. Roles of hematopoietic transcription factors GATA-1 and GATA-2 in the development of red blood cell lineage. Acta Haematol. 2002; 108(4):237-45.
19. Weiss MJ, Keller G, Orkin SH. Novel insights into erythroid development revealed through in vitro differentiation of GATA-1 embryonic stem cells. Genes Dev. 1994;8(10):1184-97.
20. Fujiwara Y, Browne CP, Cunniff K, Goff SC, Orkin SH. Arrested development of embryonic red cell precursors in mouse embryos lacking transcription factor GATA-1. Proc Natl Acad Sci USA. 1996;93(22):12355-8.
21. Surinya KH, Cox TC, May BK. Identification and characterization of a conserved erythroid-specific enhancer located in intron 8 of the human 5-aminolevulinate synthase 2 gene. J Biol Chem. 1998;273 (27):16798-809.
22. Fujiwara T, O'Geen H, Keles S, Blahnik K, Linnemann AK, Kang YA, et al. Discovering hematopoietic mechanisms through genome-wide analysis of GATA factor chromatin occupancy. Mol Cell. 2009;36(4):667-81.
23. Vargas PD, Furuyama K, Sassa S, Shibahara S. Hypoxia decreases the expression of the two enzymes responsible for producing linear and cyclic tetrapyrroles in the heme biosynthetic pathway. FEBS J. 2008;275(23): 5947-59.
24. Bekri S, May A, Cotter PD, Al-Sabah AI, Guo X, Masters GS, et al. A promoter mutation in the erythroid-specific 5-aminolevulinate synthase (ALAS2) gene causes X-linked sideroblastic anemia. Blood. 2003;102(2): 698-704.
25. Muto A, Hoshino H, Madisen L, Yanai N, Obinata M, Karasuyama H, et al. Identification of Bach2 as a B-cell-specific partner for small maf proteins that negatively regulate the immunoglobulin heavy chain gene 3' enhancer. EMBO J. 1998;17(19): 5734-43.
26. Kadirvel S, Furuyama K, Harigae H, Kaneko K, Tamai Y, Ishida Y, et al. The carboxyl-terminal region of erythroid-specific 5-aminolevulinate synthase acts as an intrinsic modifier for its catalytic activity and protein stability. Exp Hematol. 2012;40(6): 477-86 e1.
27. Szpurka H, Tiu R, Murugesan G, Aboudola S, Hsi ED, Theil KS, et al. Refractory anemia with ringed sideroblasts associated with marked thrombocytosis (RARS-T), another myeloproliferative condition characterized by JAK2 V617F mutation. Blood. 2006;108 (7):2173-81.
28. Miller IJ, Bieker JJ. A novel, erythroid cell-specific murine transcription factor that binds to the CACCC element and is related to the Kruppel family of nuclear proteins. Mol Cell Biol. 1993;13(5):2776-86.
29. Ney PA, Sorrentino BP, McDonagh KT, Nienhuis AW. Tandem AP-1-binding sites within the human beta-globin dominant control region function as an inducible enhancer in erythroid cells. Genes Dev. 1990;4(6):993-1006.
30. Harigae H, Furuyama K. Hereditary sideroblastic anemia: pathophysiology and gene mutations. Int J Hematol. 2010;92(3):425-31.
31. Ducamp S, Kannengiesser C, Touati M, Garcon L, Guerci-Bresler A, Guichard JF, et al. Sideroblastic anemia: molecular analysis of the ALAS2 gene in a series of 29 probands and functional studies of 10 missense mutations. Hum Mutat. 2011;32(6):590-7.
32. May A, Barton C, Masters G, Kingston J, Lawless S, Jenner M. Severe sideroblastic anaemia in an ALAS2 compound heterozygote for -206G, a common polymorphism, and a novel mutation in exon 11 (Lys535del) linked to lack of haemoglobinisation in vitro and ineffective erythropoiesis in vivo. Blood (ASH Annual Meeting Abstracts). 2005;106 (11):3541.
33. Dou QP, Fridovich-Keil JL, Pardee AB. Inducible proteins binding to the murine thymidine kinase promoter in late G1/S phase. Proc Natl Acad Sci USA. 1991;88(4): 1157-61.
34. Lagrange T, Kapanidis AN, Tang H, Reinberg D, Ebright RH. New core promoter element in RNA polymerase II-dependent transcription: sequence-specific DNA binding by transcription factor IIB. Genes Dev. 1998;12(1):34-44.
35. Gallagher PG, Sabatino DE, Romana M, Cline AP, Garrett LJ, Bodine DM, et al. A human beta-spectrin gene promoter directs high level expression in erythroid but not muscle or neural cells. J Biol Chem. 1999;274(10):6062-73.
36. Faisst S, Meyer S. Compilation of vertebrate-encoded transcription factors. Nucleic Acids Res. 1992;20(1):3-26.
37. Rikitake Y, Moran E. DNA-binding properties of the E1A-associated 300-kilodalton protein. Mol Cell Biol. 1992;12(6):2826-36.
38. Moser M, Imhof A, Pscherer A, Bauer R, Amselgruber W, Sinowatz F, et al. Cloning and characterization of a second AP-2 transcription factor: AP-2 beta. Development. 1995;121(9):2779-88.
39. Gilthorpe J, Vandromme M, Brend T, Gutman A, Summerbell D, Totty N, et al. Spatially specific expression of Hoxb4 is dependent on the ubiquitous transcription factor NFY. Development. 2002;129(16): 3887-99.
40. Nallur GN, Prakash K, Weissman SM. Multiplex selection technique (MuST): an approach to clone transcription factor binding sites. Proc Natl Acad Sci USA. 1996; 93(3):1184-9.
41. Sorensen KD, Quintanilla-Martinez L, Kunder S, Schmidt J, Pedersen FS. Mutation of all Runx (AML1/core) sites in the enhancer of T-lymphomagenic SL3-3 murine leukemia virus unmasks a significant potential for myeloid leukemia induction and favors enhancer evolution toward induction of other disease patterns. J Virol. 2004;78(23):13216-31.
42. Spandidos DA, Yiagnisis M, Pintzas A. Human immunodeficiency virus long terminal repeat responds to transformation by the mutant T24 H-ras1 oncogene and it contains multiple AP-1 binding TPA-inducible consensus sequence elements. Anticancer Res. 1989;9(2):383-6.
43. Mullhaupt B, Feren A, Jones A, Fodor E. DNA sequence and functional characterization of the human and rat epidermal growth factor promoter: regulation by cell growth. Gene. 2000;250(1-2):191-200.

nature genetics

Somatic *RHOA* mutation in angioimmunoblastic T cell lymphoma

Mamiko Sakata-Yanagimoto[1,22], Terukazu Enami[1,22], Kenichi Yoshida[2,3,22], Yuichi Shiraishi[4], Ryohei Ishii[5], Yasuyuki Miyake[1], Hideharu Muto[1], Naoko Tsuyama[6], Aiko Sato-Otsubo[2,3], Yusuke Okuno[2], Seiji Sakata[7], Yuhei Kamada[1], Rie Nakamoto-Matsubara[1], Nguyen Bich Tran[1], Koji Izutsu[8,9], Yusuke Sato[2,3], Yasunori Ohta[10], Junichi Furuta[11], Seiichi Shimizu[12], Takuya Komeno[13], Yuji Sato[14], Takayoshi Ito[15], Masayuki Noguchi[16], Emiko Noguchi[17], Masashi Sanada[2,3], Kenichi Chiba[4], Hiroko Tanaka[18], Kazumi Suzukawa[1,19], Toru Nanmoku[19], Yuichi Hasegawa[1], Osamu Nureki[5], Satoru Miyano[4,18], Naoya Nakamura[20], Kengo Takeuchi[6,7], Seishi Ogawa[2,3,23] & Shigeru Chiba[1,21,23]

Angioimmunoblastic T cell lymphoma (AITL) is a distinct subtype of peripheral T cell lymphoma characterized by generalized lymphadenopathy and frequent autoimmune-like manifestations[1,2]. Although frequent mutations in *TET2*, *IDH2* and *DNMT3A*, which are common to various hematologic malignancies[3,4], have been identified in AITL[5–8], the molecular pathogenesis specific to this lymphoma subtype is unknown. Here we report somatic *RHOA* mutations encoding a p.Gly17Val alteration in 68% of AITL samples. Remarkably, all cases with the mutation encoding p.Gly17Val also had *TET2* mutations. The *RHOA* mutation encoding p.Gly17Val was specifically identified in tumor cells, whereas *TET2* mutations were found in both tumor cells and non-tumor hematopoietic cells. *RHOA* encodes a small GTPase that regulates diverse biological processes. We demonstrated that the Gly17Val RHOA mutant did not bind GTP and also inhibited wild-type RHOA function. Our findings suggest that impaired RHOA function in cooperation with preceding loss of TET2 function contributes to AITL-specific pathogenesis.

AITL accounts for approximately 20% of all T cell lymphoma cases[1]. On the basis of gene expression profiling, the normal counterparts of AITL tumor cells are proposed to be follicular helper T cells (T_{FH} cells), a subset of helper T cells[1,2]. Peripheral T cell lymphoma, not otherwise specified (PTCL-NOS) represents a more heterogeneous category of mature T cell lymphomas, including a subset sharing some features of AITL[5,9].

To explore the relevant gene mutations responsible for the pathogenesis of AITL, we performed whole-exome sequencing[10] of three AITL and three PTCL-NOS samples (**Supplementary Table 1**). Of the targeted sequence, 86.5% was analyzed by ≥20 independent reads on average (**Supplementary Figs. 1** and **2**). In total, we identified and confirmed 87 non-silent somatic mutations (4–27 (median of 12.5) per sample) by Sanger sequencing and/or deep sequencing (**Fig. 1a** and **Supplementary Table 2**), including 79 missense and 5 nonsense single-nucleotide variants (SNVs) and 1 non-frameshift and 2 frameshift deletions. The numbers of non-silent mutations were lower than reported in B cell neoplasms[11,12], although relatively low tumor contents, which were suspected owing to mutant allele frequencies of generally less than 0.25 (median of 0.11), could have compromised sensitivity in detecting mutations (**Fig. 1a**). Recurrent mutations were found in only one gene, *RHOA*, in which identical c.50G>T mutations predicted to result in a p.Gly17Val alteration were identified in one PTCL-NOS and three AITL specimens (**Fig. 1a,b** and **Supplementary Fig. 3**). No allelic imbalances were observed at the *RHOA* locus (**Supplementary Fig. 4**).

Prompted by this discovery, we screened *RHOA* mutations in an extended cohort of 72 AITL and 87 PTCL-NOS samples by

[1]Department of Hematology, Faculty of Medicine, University of Tsukuba, Tsukuba, Japan. [2]Cancer Genomics Project, Graduate School of Medicine, The University of Tokyo, Tokyo, Japan. [3]Department of Pathology and Tumor Biology, Graduate School of Medicine, Kyoto University, Kyoto, Japan. [4]Laboratory of DNA Information Analysis, Human Genome Center, Institute of Medical Science, The University of Tokyo, Tokyo, Japan. [5]Department of Biophysics and Biochemistry, Graduate School of Science, The University of Tokyo, Tokyo, Japan. [6]Division of Pathology, Cancer Institute, Japanese Foundation for Cancer Research, Tokyo, Japan. [7]Pathology Project for Molecular Targets, Cancer Institute, Japanese Foundation for Cancer Research, Tokyo, Japan. [8]Department of Hematology, Toranomon Hospital, Tokyo, Japan. [9]Okinaka Memorial Institute for Medical Research, Tokyo, Japan. [10]Department of Pathology, Toranomon Hospital, Tokyo, Japan. [11]Department of Dermatology, Faculty of Medicine, University of Tsukuba, Tsukuba, Japan. [12]Department of Hematology, Tsuchiura Kyodo General Hospital, Tsuchiura, Japan. [13]Department of Hematology, Mito Medical Center, National Hospital Organization, Mito, Japan. [14]Department of Hematology, Tsukuba Memorial Hospital, Tsukuba, Japan. [15]Department of Hematology, JA Toride Medical Center, Toride, Japan. [16]Department of Pathology, Faculty of Medicine, University of Tsukuba, Tsukuba, Japan. [17]Department of Medical Genetics, Faculty of Medicine, University of Tsukuba, Tsukuba, Japan. [18]Laboratory of Sequence Analysis, Human Genome Center, Institute of Medical Science, The University of Tokyo, Tokyo, Japan. [19]Department of Clinical Laboratory, University of Tsukuba Hospital, Tsukuba, Japan. [20]Department of Pathology, Tokai University School of Medicine, Isehara, Japan. [21]Life Science Center, Tsukuba Advanced Research Alliance, University of Tsukuba, Tsukuba, Japan. [22]These authors contributed equally to this work. [23]These authors jointly directed this work. Correspondence should be addressed to S.C. (schiba-t@md.tsukuba.ac.jp) or S.O. (sogawa-tky@umin.ac.jp).

Received 13 May 2013; accepted 12 December 2013; published online 12 January 2014; doi:10.1038/ng.2872

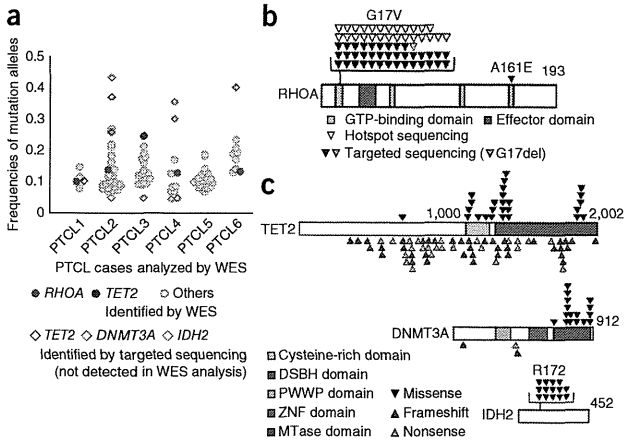

Figure 1 Discovery of a *RHOA* mutation encoding p.Gly17Val in PTCL by whole-exome sequencing. (**a**) Somatic mutations identified in three AITL and three PTCL-NOS samples are shown with the frequencies of mutation alleles plotted. Red and blue filled circles indicate the *RHOA* mutation encoding p.Gly17Val and *TET2* mutations, respectively. Mutations of *TET2*, *IDH2* and *DNMT3A* that were not found by whole-exome sequencing (WES) but were identified later by targeted deep sequencing are also depicted by open diamonds: blue, *TET2*; orange, *DNMT3A*; purple, *IDH2*. (**b**) Positions of RHOA alterations. Nucleotide-binding domains are represented by yellow boxes. The effector domain is represented by a red box. (**c**) Positions of alterations in the TET2, DNMT3A and IDH2 proteins. Black, red and yellow arrowheads indicate missense, frameshift and nonsense mutations, respectively. The cysteine-rich and double-strand β-helix (DSBH) domains of TET2 are represented by a yellow and a red box, respectively. proline-tryptophan-tryptophan-proline (PWWP), zinc-finger (ZNF) and methyltransferase (MTase) domains of DNMT3A are shown by light blue, blue and purple boxes, respectively.

deep sequencing of all coding sequences (n = 79) or the mutational hotspot (c.50G>T; p.Gly17Val) (n = 80) of *RHOA* (**Supplementary Fig. 1** and **Supplementary Table 3**). *RHOA* mutations were found in 66 of the 159 specimens, with a much higher frequency in AITL (51/72; 70.8%) than PCTL-NOS (15/87; 17.2%) (**Fig. 1b**, **Table 1** and **Supplementary Table 4**). We identified no *RHOA* mutations other than the c.50G>T (p.Gly17Val) mutation except for an in-frame deletion (c.49_51delGGA) resulting in a p.Gly17del (PTCL33) alteration and a missense SNV (c.482C>A) resulting in a p.Ala161Glu (PTCL59) alteration in cases negative for the p.Gly17Val alteration (**Fig. 1b** and **Supplementary Table 4**). We validated all low-frequency mutant *RHOA* alleles (frequency of 0.02–0.05) using an independent deep sequencing platform (Online Methods). No *RHOA* mutations encoding p.Gly17Val were found in other hematologic malignancies, including in myeloid neoplasms (n = 142), mature B cell neoplasms (n = 91) and mature T cell neoplasms other than AITL and PTCL-NOS (n = 11) (**Table 1**), suggesting that the *RHOA* mutation encoding p.Gly17Val is highly specific to AITL and PTCL-NOS among hematologic malignancies.

According to the pathologic definition in the Online Methods[5,9], we classified 21 of 59 immunohistochemically characterized PTCL-NOS cases as T_{FH}-like PTCL-NOS cases. Thirteen of the 21 T_{FH}-like PTCL-NOS cases (61.9%) had the *RHOA* mutation encoding p.Gly17Val, whereas none of the remaining 38 PTCL-NOS cases had this mutation ($P < 0.001$) (**Supplementary Table 5**). Given that almost all AITL cases showed T_{FH}-like features, these findings implied a strong correlation between the *RHOA* mutation encoding p.Gly17Val and the T_{FH}-like phenotype of PTCL, similar to the correlation previously shown between *TET2* mutations and the T_{FH}-like phenotype of PTCL[5]. No clinical parameters were significantly different in the mutation-positive and mutation-negative cases (**Supplementary Fig. 5** and **Supplementary Table 6**).

To investigate the correlation between mutations in *RHOA* and other genes, we also resequenced *TET2*, *IDH1*, *IDH2* and *DNMT3A* in addition to *RHOA* in the subcohort of 79 PTCL (AITL, 46; PTCL-NOS, 33) cases (**Supplementary Figs. 1** and **6**). A total of 97 *TET2* mutations were identified in 54 of the 79 PTCL specimens (68.4%) (AITL, 38 (82.6%); PTCL-NOS, 16 (48.5%)). Similarly, we found *DNMT3A* mutations in 21 PTCL specimens (26.6%) (AITL, 12 (26.0%); PTCL-NOS, 9 (27.3%)). We identified *IDH2* mutations affecting Arg172 (p.Arg172Met, p.Arg172Thr, p.Arg172Ser, p.Arg172Lys and p.Arg172Gly) in 14 cases (17.7%) (AITL, 14 (30.4%); PTCL-NOS, 0 (0%)) (**Figs. 1c** and **2a**, **Supplementary Tables 7** and **8**, and **Supplementary Note**). No *IDH1* mutations were identified. Several mutations in *TET2*, *IDH2* and *DNMT3A*, which had escaped detection in the whole-exome sequencing analysis, were newly identified in the same whole-exome sequencing cohort by this targeted resequencing. Our inability to detect these mutations using whole-exome sequencing might be explained by their low allelic mutational burdens and/or by low sequencing coverage in whole-exome sequencing (**Fig. 1a**). Unexpectedly, however, *TET2* and *DNMT3A* mutations with high-frequency alleles were also newly found in three and two cases, respectively (**Fig. 1a**). The cause of our inability to identify *TET2* and *DNMT3A* mutations by whole-exome sequencing might be the presence of substantial numbers of mutant reads in the reference bone marrow samples (**Supplementary Fig. 7**, **Supplementary Tables 9** and **10**, and **Supplementary Note**).

Remarkably, mutations in *RHOA*, *TET2* and *IDH2* showed strong correlations; all *RHOA*-mutated cases also had *TET2* mutations ($P < 0.001$), and all but one of the *IDH2* mutations were confined to tumors also having *RHOA* and *TET2* mutations ($P < 0.001$) (**Fig. 2a** and **Supplementary Note**). The predominant *TET2* alleles showed significantly higher allelic burden than mutant *RHOA* and *IDH2* alleles in most cases (*TET2* versus *RHOA*, $P < 0.001$; *TET2* versus *IDH2*, $P = 0.001$; **Fig. 2b,c**), whereas *RHOA* and *IDH2* mutations had similar allele frequencies (**Fig. 2d**). Skewed distributions of relative allele frequencies among these mutations strongly suggested that *TET2* mutations predated *RHOA* and/or *IDH2* mutations in most cases.

Table 1 *RHOA* mutation encoding p.Gly17Val in various hematologic malignancies

Disease	Number of mutated cases (%)
T cell malignancies	n = 170
AITL[a]	51/72 (70.8)
PTCL-NOS	15/87 (17.2)
with AITL features	13/21 (61.9)
without AITL features	0/38 (0)
ND[b]	2/28 (7.1)
Other T cell malignancies	0/11 (0)
B cell malignancies	n = 91
DLBCL	0/44 (0)
Follicular lymphoma	0/19 (0)
Other B cell malignancies	0/28 (0)
Myeloid malignancies	n = 142
AML	0/89 (0)
MDS	0/36 (0)
MPN	0/14 (0)
MDS/MPN	0/3 (0)

DLBCL, diffuse large B cell lymphoma; AML, acute myeloid leukemia; MDS, myelodysplastic syndrome; MPN, myeloproliferative neoplasm.
[a]Including one case with RHOA p.Gly17del and one case with RHOA p.Ala161Glu.
[b]Not determined.

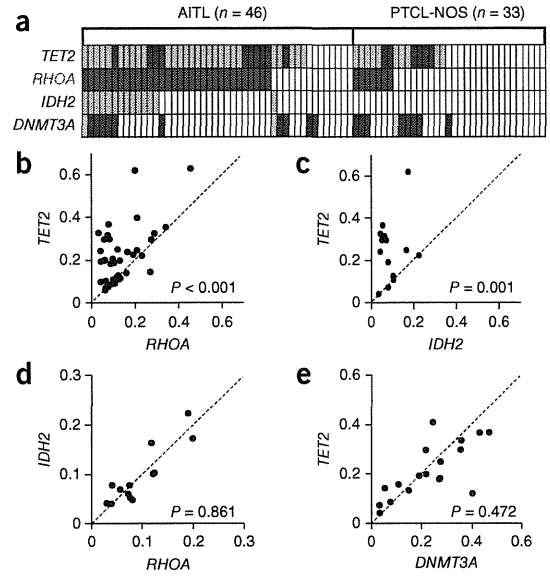

Figure 2 Relationship between *RHOA*, *TET2*, *IDH2* and *DNMT3A* mutations in PTCL. (**a**) Distribution of mutations in *RHOA*, *TET2*, *IDH2* and *DNMT3A* in 79 PTCL (46 AITL and 33 PTCL-NOS) samples that were analyzed by targeted deep sequencing. Two or three distinct *TET2* mutations and two distinct *DNMT3A* mutations were identified in multiple samples. Dark blue and dark green indicate samples having a single *TET2* or *DNMT3A* mutation, respectively, and light blue and light green indicate samples having multiple *TET2* or *DNMT3A* mutations. (**b–e**) Comparison of the allele frequencies of two selected mutations in samples harboring mutations in *TET2* and *RHOA* (**b**), *TET2* and *IDH2* (**c**), *RHOA* and *IDH2* (**d**) and *TET2* and *DNMT3A* (**e**). Each axis shows the frequencies of the mutant alleles. When multiple mutations existed in a single gene, the frequencies of major alleles are indicated. Data were analyzed statistically by Wilcoxon rank-sum test.

Mutations in *DNMT3A* largely overlapped and had similar allelic burdens as *TET2* mutations (**Fig. 2e**), but their correlation with *RHOA* or *IDH2* mutations was much less clear (**Fig. 2a**).

To determine the clonal structure of the *RHOA* mutation encoding p.Gly17Val and of other gene mutations, we isolated CD4$^+$ T cells, a fraction enriched for tumor cells and other fractions, from the specimens of two cases (PTCL159 and PTCL160; **Supplementary Figs. 8** and **9**), and we analyzed mutations by targeted resequencing as well as by Sanger sequencing. In PTCL159 (PTCL-NOS in the skin), we found the *RHOA* mutation encoding p.Gly17Val, two *TET2* mutations and a *DNMT3A* mutation (**Supplementary Fig. 8** and **Supplementary Table 7**). Somatic origin of these mutations was confirmed (**Supplementary Fig. 8**). We identified the *RHOA* mutation encoding p.Gly17Val in purified CD4$^+$ cells but not in CD8$^+$ cells. One of the two *TET2* mutations and the *DNMT3A* mutation were identified in both CD4$^+$ and CD8$^+$ cell fractions with apparently similar allelic burdens to each other in the two types of cells, whereas the remaining *TET2* mutation was found only in CD4$^+$ cells and was absent in CD8$^+$ cells (**Supplementary Fig. 8**). These observations suggested that the *RHOA* mutation encoding p.Gly17Val and one of the two *TET2* mutations were confined to CD4$^+$ tumor cells, whereas the other *TET2* mutation and the *DNMT3A* mutation were shared by both CD4$^+$ tumor cells and CD4$^+$ and CD8$^+$ reactive cells (**Supplementary Fig. 8**). In contrast, the *RHOA* mutation encoding p.Gly17Val and two *TET2* mutations identified in PTCL160 (AITL) were all confined to tumor cells (**Supplementary Fig. 9**, **Supplementary Table 7** and **Supplementary Note**). These data indicate that the *RHOA* mutation encoding p.Gly17Val was a specific event in tumor cells. In contrast, *TET2* and *DNMT3A* mutations seemed to have taken place in either CD4$^+$ tumor cells or early progenitor cells such as those that give rise to all hematopoietic cells, as previously described[6,7].

RHOA encodes a small GTPase, which has a highly conserved amino acid structure across species (**Supplementary Fig. 10**). RHOA operates as a molecular switch that regulates a wide variety of biological processes through cycling between an active (GTP-bound) state and an inactive (GDP-bound) state[13,14]. RHOA is activated by specific guanine-exchange factors (GEFs) that catalyze the dissociation of GDP and the rebinding of GTP, and signaling is terminated by hydrolysis of GTP to GDP, a reaction that is stimulated by GTPase-activating proteins (GAPs)[13,14].

Three-dimensional model structures of the Gly17Val RHOA protein suggest compromised binding to GDP and GTP[15,16] (**Supplementary Fig. 11** and **Supplementary Note**). In fact, when we expressed RHOA proteins in NIH3T3 cells, a substantial fraction of wild-type RHOA protein bound GTP or GTPγS in a rhotekin pulldown assay[17], whereas no GTP- or GTPγS-bound form was pulled down for the Gly17Val RHOA mutant (**Fig. 3a**), suggesting severely reduced GTP and GTPγS binding by the Gly17Val mutant.

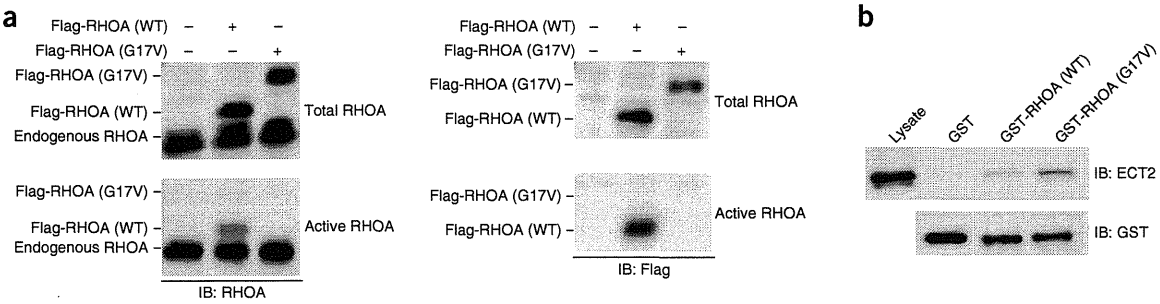

Figure 3 Dominant-negative effect of the Gly17Val RHOA mutant on wild-type RHOA. (**a**) Rhotekin pulldown assay for endogenous RHOA and exogenously expressed wild-type and Gly17Val RHOA in NIH3T3 cells. Extracts from NIH3T3 cells expressing Flag-tagged wild-type or Gly17Val RHOA were pulsed with GTPγS and incubated with glutathione Sepharose beads on which the RHO-binding domain of rhotekin fused to GST was immobilized, and precipitated protein was blotted with antibodies to RHOA (left) and Flag (right) to detect active RHOA specifically. IB, immunoblot; WT, wild type. (**b**) GEF-binding activity of wild-type and Gly17Val RHOA. Lysate from NIH3T3 cells, transiently expressing ECT2 with an N-terminal deletion, was incubated with Sepharose beads on which GST-fused wild-type or Gly17Val RHOA protein was immobilized, and precipitated protein was blotted with antibody to ECT2.

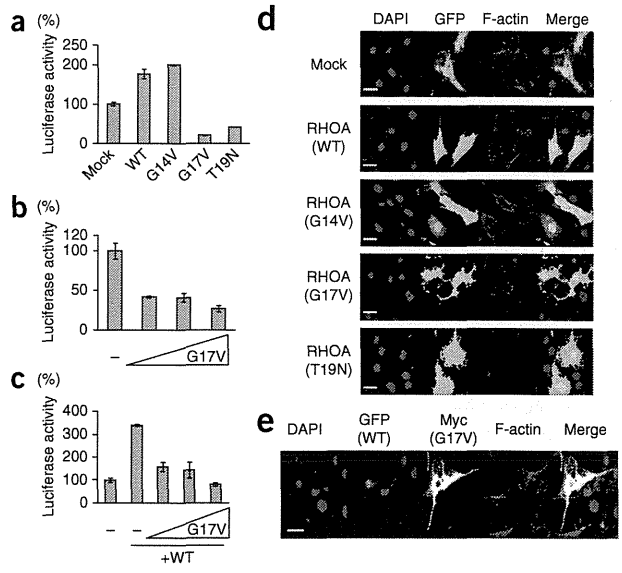

Figure 4 Effects of the Gly17Val RHOA mutant on transcriptional regulation and actin cytoskeleton formation in NIH3T3 cells. (**a–c**) Effect of Gly17Val RHOA on the transcriptional activity of the SRF-RE. (**a**) Activity of the SRF-RE reporter in NIH3T3 cells expressing wild-type or mutant (Gly14Val, Gly17Val or Thr19Asn) RHOA protein. (**b**) Effect of increasing amounts (16, 48 or 144 ng/well) of Gly17Val RHOA on SRF-RE reporter activity in NIH3T3 cells. (**c**) Effect of increasing amounts (16, 48 or 144 ng/well) of Gly17Val RHOA on SRF-RE reporter activity enhanced by exogenously expressed wild-type RHOA. In each plot in **a–c**, the mean ± s.d. of triplicate experiments is shown. A representative result from three independent experiments is shown. (**d,e**) Effect of Gly17Val RHOA on actin cytoskeleton formation. (**d**) F-actin staining with phalloidin (red) in NIH3T3 cells transiently transfected with vector expressing wild-type or mutant (Gly14Val, Gly17Val or Thr19Asn) RHOA. GFP is used as a marker for transduction with each cDNA. (**e**) NIH3T3 cells stably expressing wild-type RHOA were transfected with vector expressing Myc-tagged Gly17Val RHOA. Scale bars in **d,e**, 30 μm.

Moreover, the Gly17Val RHOA mutant reduced GTP binding by both the endogenous and exogenous wild-type RHOA proteins in a dose-dependent manner (**Supplementary Figs. 12** and **13**), suggesting a dominant-negative nature for Gly17Val RHOA. This view was further supported by the finding that the Gly17Val RHOA mutant bound ECT2, one of the RhoGEFs, more tightly than wild-type RHOA, as was previously described for Gly17Ala RHOA[18] (**Fig. 3b** and **Supplementary Note**). The Gly17del and Ala161Glu mutants also showed impaired binding capacity for GTP/GTPγS and inhibited GTP binding by wild-type RHOA protein (**Supplementary Fig. 14**). Together, these results support the notion that the RHOA mutants contribute to the pathogenesis of PTCL through the inhibition of wild-type RHOA in a dominant-negative manner, although the amount of mutant RHOA protein seemed to be low in both NIH3T3 cells and primary AITL tumor cells (**Supplementary Fig. 15**, **Supplementary Table 11** and **Supplementary Note**), for an unknown reason.

In accordance with these findings, unlike wild-type RHOA and mutant Gly14Val RHOA, the Gly17Val RHOA mutant did not activate transcription from the serum response factor–responsive element (SRF-RE)[19] (**Fig. 4a,b**) and instead repressed transcription from SRF-RE activated by exogenously expressed wild-type RHOA (**Fig. 4c**), as did a known dominant-negative mutant of RHOA (Thr19Asn) (**Fig. 4a** and data not shown). Gly17Val as well as Thr19Asn RHOA also attenuated actin stress fiber formation in NIH3T3 cells, which was markedly induced by wild-type and Gly14Val RHOA[20] (**Fig. 4d**). Furthermore, the Gly17Val RHOA mutant inhibited the assembly of actin stress fibers in NIH3T3 cells stably expressing wild-type RHOA (**Fig. 4e**). All these data suggest that the Gly17Val mutant functions in a dominant-negative manner with respect to wild-type RHOA.

To investigate the effect of wild-type and Gly17Val RHOA on T cells, we established Jurkat cells inducibly expressing wild-type or Gly17Val RHOA (**Fig. 5a**). When wild-type RHOA was expressed, the proliferation of Jurkat cells was significantly decreased (WT Dox (+) versus Mock DOX (+), $P < 0.001$, days 2–4; **Fig. 5b**), and G1-to-S cell cycle progression was suppressed (**Supplementary Fig. 16**). In contrast, inducibly expressed Gly17Val RHOA did not affect the growth or cell cycle progression of Jurkat cells (**Fig. 5b** and **Supplementary Fig. 16**). We further performed mRNA sequencing analysis to examine the effect of the *RHOA* mutation encoding p.Gly17Val on gene expression, using RNA prepared from Jurkat cells inducibly expressing wild-type or Gly17Val RHOA or mock-transfected cells, as well as RNA from NIH3T3 cells transiently expressing wild-type or Gly17Val RHOA or mock-transfected cells. Gene Set Enrichment Analysis (GSEA)[21,22] demonstrated that the serum response factor (SRF) pathway, known to be activated under RHOA signaling[23], was significantly enriched at a false discovery rate (FDR) q value less than 0.25 for cells expressing wild-type RHOA versus mock-transfected cells in both Jurkat and NIH3T3 cells

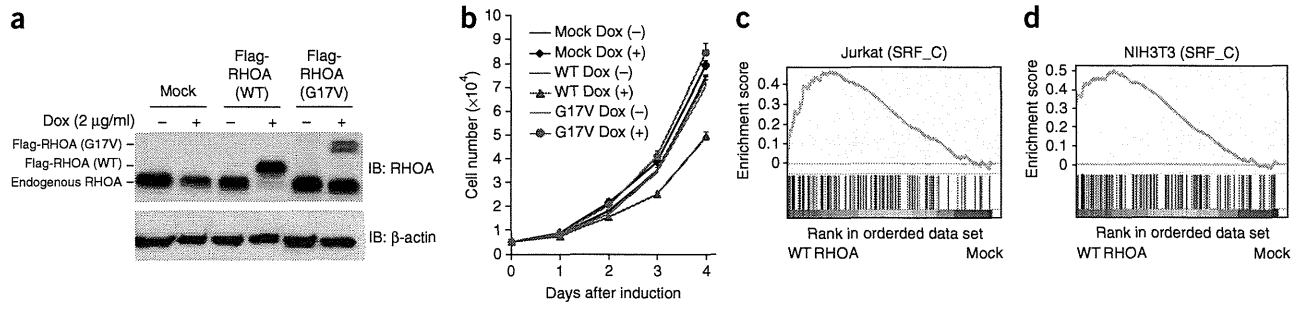

Figure 5 Effect of Gly17Val RHOA on T cells. (**a**) Doxycycline (Dox)-induced expression of wild-type and Gly17Val RHOA in Jurkat cells. A protein blot with antibody to RHOA is shown. β-actin is used as a loading control. (**b**) Proliferation of Jurkat cells inducibly expressing wild-type or Gly17Val RHOA. Absorbance (at 450 nm) was converted to cell number. The mean ± s.d. of quadruplicate experiments is shown. A representative result from three independent experiments is shown. (**c,d**) GSEA for Jurkat cells inducibly expressing wild-type or Gly17Val RHOA or mock transfected and NIH3T3 cells transiently expressing wild-type or Gly17Val RHOA or mock transfected ($n = 2$ each). The SRF pathway was differentially enriched in both Jurkat cells (**c**) and NIH3T3 cells (**d**). SRF_C refers to the V$SRF_C gene set.